Journal of
Mechanics of
Materials and Structures

EFFECTIVE PROPERTY ESTIMATES FOR HETEROGENEOUS MATERIALS WITH COCONTINUOUS PHASES

Patrick Franciosi, Renald Brenner and Abderrahim El Omri

Volume 6, No. 5 May 2011

mathematical sciences publishers

JOURNAL OF MECHANICS OF MATERIALS AND STRUCTURES
Vol. 6, No. 5, 2011

EFFECTIVE PROPERTY ESTIMATES FOR HETEROGENEOUS MATERIALS WITH COCONTINUOUS PHASES

PATRICK FRANCIOSI, RENALD BRENNER AND ABDERRAHIM EL OMRI

This work concerns heterogeneous multiphase materials which may exhibit omnidirectional full or partial cocontinuity of several or all phases. The estimate of their effective (mechanical or physical) properties is not yet well handled as compared to those for well-defined aggregate or reinforced-matrix structures, especially in the context of homogenization methods. We propose in this framework a modeling scheme which aims at accounting for such phase cocontinuity features. In the mechanical application field, the modeling validity restricts to elastic properties of unloaded materials or in load situations as far as bending and torsion effects of possibly strut-like phase parts are not essential. For other physical properties (dielectric, magnetic, etc.), the modeling applications concern those for which homogenization approaches are relevant. The modeling is based on a material's morphology description in terms of a generalization of so-called "fiber systems" that were introduced in early literature reports. Using parameters that describe the clustering characteristics of the individual phases and of their assemblage, we have considered these fiber systems both within a layer-based approach of the material structure and within an aggregate-like one. By these two routes, we have obtained two estimate forms that differ only slightly in definition. The presentation uses the elasticity formalism, in simple cases of isotropic mixtures of two-phase materials with isotropic phase behavior but the modeling extends to n-phase anisotropic materials as established separately. Our estimates are compared with basic variational bounds and homogenization estimates, with some literature data and with homogenization results obtained with the fast Fourier transform approach on numerical structures. All data are matched with different parameter sets corresponding to different types of phase organization. The two estimates remain nearly equal for all of the examined structures regardless of phase contrast and with only slight differences consistent with their definition difference.

1. Introduction

The continuity of a phase in a material here means the existence of an infinite (or sample spanning) cluster of that phase in the material with regard to one, several or all directions of space. Although this phase continuity is sometimes called phase percolation, this latter term is the most often related to the transition threshold between discontinuity and continuity. In that respect, phase cocontinuity is to be understood as the coexistence of multidirectional sample spanning clusters from different phases. Multiphase materials with cocontinuous phases, to be called cocontinuous materials for short, are of many different structure types: sponge-like structures, bones, blends, foams, braided composites, etc. These structures, named from porous examples, can also characterize assemblages of several solid phases. They can be made of ceramics, polymers, metals, biomaterials and composites of these. A wide variety of interesting physical and mechanical properties make the experimental investigations of their effective properties increasing

Keywords: phase cocontinuity, effective properties, heterogeneous materials, clustering.

fast [Nieh et al. 1998; Veenstra et al. 2000; La Vecchia et al. 2003; Morgan et al. 2003; Agrawal et al. 2003; Kinney et al. 2005; Marur 2005]. Yet it is not easy to find data sets that allow the relation of their overall properties with the specific features of their phase arrangements.

On the theoretical ground, insights into aggregates and particle- (or fiber-) reinforced composites have been considerable during the last decades, themselves based on a set of pioneering works [Hill 1952; Hill 1965; Kerner 1956; Boucher 1974; Walpole 1978; 1981; Christensen 1979a; 1979b; Hashin 1979; 1983], in the context of homogenization theory especially. Well defined frameworks have been provided for composite materials that exhibit phase cocontinuity with regard to only one direction (parallel fibers) or two directions (laminate structures) in space and omnidirectional cocontinuity has been explored using some ideal structures such as the overlapping sphere models; see for example [Berryman 1985]. Yet, estimates of effective elastic, electric or other properties for (isotropic or not) materials with multidirectionally cocontinuous phases have not been the matter of many examinations in this homogenization context.

In counterpart, many models derived for cocontinuous materials, are based on rheological descriptions combining series and parallel arrangements of the phases [Ravichandran 1994; Fan 1995; Leßle et al. 1999; Dalmaz et al. 2000]. Also, a lot of works make use of finite element methods or other computational techniques based on meshing or space-partitioning procedures [Feng et al. 2003; Chen et al. 2008]. Numerical homogenization techniques provide as well relevant estimates applicable to various effective properties [Roberts and Garboczi 2002; Delannay et al. 2006; Pavese et al. 2007].

Specific models have been developed for the particular mechanical properties exhibited by some of these cocontinuous materials as the cellular materials or some open cell foams, in order to account for bending and torsion characteristics, due to strut-like elements [Gent and Thomas 1959; Ko 1965; Menges and Knipschild 1975; Warren and Kraynik 1987; 1997]. These effects are partly handled in numerical modeling, they are not in rheological ones and they would not be at all in a homogenization approach. Widely used specific models as the Kelvin cell model [Gong et al. 2005] or also some systematic statistical approaches are also dedicated to these particular mechanical characteristics [Berk 1987; Roberts and Garboczi 2002].

But materials with cocontinuous phases are of very many different types and their mechanical behavior does not necessarily exhibit such particular mechanical characteristics. Furthermore, materials in their unloaded state have intrinsic elastic properties worth to be known if accessible. Experimental information for the unloaded state can be obtained for example from laser ultrasonic probing or from the extrapolation at zero strain of elastic data from the unloading stage of mechanical tests [Lefebvre et al. 2006].

In spite of this quite large variety of proposed models, in proportion to the variety of structures, it is frequently stated in the concerned literature that the obtained fit with measurements remains limited with regard to either mechanical or physical overall properties.

From these considerations, the goal of the present work is to formulate, in the context of homogenization methods, a modeling scheme to estimate the effective properties of multiphase materials which allows to account for a wide diversity of phase cocontinuity situations, partial or total, symmetrically for the concerned phases or not, etc. The proposed modeling is compared with available data and with direct estimates on numerically built structure by using the recent technique of fast Fourier transforms [Moulinec and Suquet 1998; Michel et al. 2001; Lebensohn et al. 2008] which provides an efficient tool for computing the properties of arbitrarily complex periodic structures. Our proposed modeling

scheme is built such as to remain consistent with the possible coexistence of one omnidirectional infinite (sample spanning) cluster of each phase present in the material. It is based on a description of the material structure from a generalization of the fiber systems introduced in [Christensen and Waals 1972] as typical examples of cocontinuous phase arrangements with regard to all directions in space. The generalized fiber systems that can be defined from a set of phases (taking, in turn, each phase as a fiber-reinforced matrix) are in a second step combined within either a layer-based approach or within an aggregate-like one of the material structure, by using parameters which describe the phase clustering characteristics for each phase individually and for their assemblage.

Regarding the employed terminology in this two-scale modeling scheme, we refer to layer-based approaches for the homogenization methods that involve models for laminate structures and to aggregate-like approaches for the methods that make use of a self-consistent modeling. The choice of considering first fiber systems in combination with a layer-based approach has been motivated by the fact that such linear and planar cuts of materials are key elements for the 3D reconstruction methods in tomography analyses [Natterer 1986] as well as for the calculation of the main lower-order "microstructural descriptors"[1] [Torquato 2002]. Secondly, aggregate-like organizations of the same representative domains have also been considered for comparison purposes with the self-consistent property estimates and also because aggregates likely have a concentration range of phase cocontinuity when the phases are in limited number and in comparable concentrations. These two modeling routes that we have explored, without loss of generality, for two-phase materials of isotropic structure and properties and which is presented in the case of the elasticity formalism although they are both holding for many other properties, yield quite similar estimate forms and definitions. They are shown to provide very close moduli estimates in situations of significant phase cocontinuity, while for vanishing cocontinuity a slight estimate difference results from the slight difference in their definitions. It is at last worth to stress that the isotropic platelet and fiber systems here considered for two-phase isotropic materials extend (as aggregate structures) to n-phase materials with possibly anisotropic phase properties and spatial arrangements. Some of their remarkable characteristics here stressed and used extend accordingly, what is presented in [Franciosi and El Omri 2011].

Section 2 introduces the considered structures and the phase continuity characteristics to be accounted for. Section 3 summarizes the fundamentals of the layer-based and aggregate-like approaches of heterogeneous materials properties and presents the estimate forms that we have worked with. Section 4 presents in the fully isotropic case the phase cocontinuity description and the morphology-based phase continuity parameters which have been introduced in the estimate formulation. Section 5 reports the result comparisons with variational bounds and homogenization estimates, with some literature data and with calculations by fast Fourier transform (FFT) numerical scheme on 3D structures with various phase cocontinuity situations.

2. Typical cocontinuous two-phase structures and phase continuity characteristics

Examples of concerned structures by the proposed modeling are collected in Figure 1. The most typical ones are the two-phase blend or sponge-like structure, Figure 1a (aluminum from [Nieh et al. 1998])

[1] N-points and surface correlation functions, lineal path function, chord-length density function, particle pair correlation function, etc. Note that the two-point correlation function also contains the two-point cluster function.

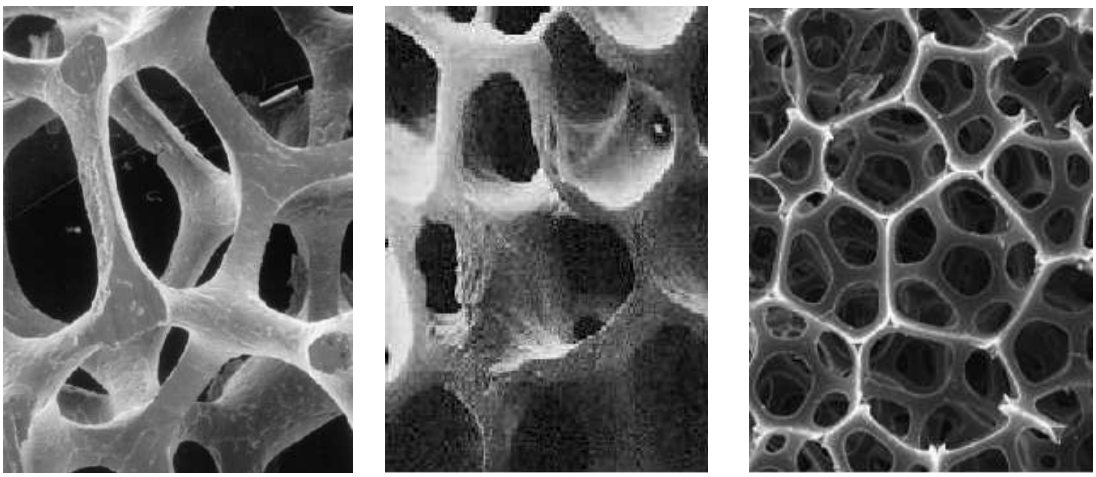

Figure 1. Examples of cocontinuous structures of concern: (a) sponge-like metallic oxide, (b) trabecular bone tissue, (c) cellular foam.

and the structure of trabecular bones, Figure 1b [Mow and Huiskes 2004], where the void volume in the exemplified materials, which can be replaced by a second solid material phase (alumina in aluminum, [La Vecchia et al. 2003], or marrow in bones), is also a continuous phase. The previously pointed importance of bending and torsion effects due to strut elements in open foam structures such as illustrated in Figure 1c [Gong et al. 2005] restricts for these materials the mechanical field of application of the proposed modeling to estimating the elastic properties either in the unloaded state of the material or in the loading situations on it when these effects are not essential.

Now, for these structures the phase cocontinuity is omnidirectional, say multidirectional in a continuous manner, either isotropically or possibly obeying some other global symmetry. There are also cocontinuous materials for which the phase cocontinuity is multidirectional but only concerns a discrete set of directions, as tubular systems and woven or weaved composites. In these architectures the mechanical features as flexibility, bending, torsion, etc can also be important. If they are not of concern here, it is worth to mention that particular arrangements of discrete direction sets for phase cocontinuity can ensure isotropic effective properties, a point to be of use in the discussions to come.

With regard to phase concentrations, many materials as polymer blends or aggregates with a limited phase number are very likely phase cocontinuous in the intermediate phase concentration range, but a dilute phase "naturally" adopts the embedded condition in general[2]. While many composites have no concentration range of phase cocontinuity (as typically glass inclusions in a polymer matrix), real n-phase structures that remain cocontinuous over the whole phase concentration range are quite scarce, if any, even for only two phases. Indeed, this would require for each of the assembled phases the existence of a continuous reinforcement down to an infinitesimal concentration of this phase. It is an advantage of numerical structures to possibly mix two phases in bicontinuous arrangements down to a nearly zero concentration, with the only limit being the chosen voxel density in a unit cell.

[2]Two-phase metals are also multiphase in terms of grain orientation distributions or crystallographic textures [Bretheau et al. 1988; Kocks et al. 1991; Lebensohn et al. 2008].

Now, the structures that would be cocontinuous over the whole phase concentration range or only over a part of it can exhibit a variety of phase cocontinuity characteristics that are specific for each material phase and likely vary with their relative phase concentrations. We have restricted attention to the materials which can be taken as isotropic and statistically homogeneous at the different length scales that we may have to successively consider. The main phase continuity characteristics to which attention is paid are (i) the amount of phase continuity, from null to total, exhibited by each material phase and (ii) the asymmetry of the cocontinuity between the material phases. For structures whose phase concentration can be varied, attention is also paid to the possible concentration dependency of these characteristics.

(1) An isotropic, cocontinuous, two-phase material contains by definition, for each phase and in an intricate manner, one multidirectionally infinite (sample-spanning) cluster possibly having "dead branches" and possibly coexisting with finite clusters that do not contribute to the phase continuity. In that respect the continuity of a phase can be said to be total when no dead branches and no finite clusters remain, and it can be said to be partial otherwise. So it is as well for phase cocontinuity: it can be said total (resp. partial) when all the cocontinuous phases are totally (resp. partially) continuous.

(2) The asymmetry of continuity between the phases can match any intermediate between perfect symmetry and the extreme situations of null cocontinuity when one of the phases totally embeds the other one(s). These latter cases correspond to the widely met and examined reinforced-matrix structures [DeBartolo and Hillberry 1998; Estevez et al. 1999; Martin et al. 2003; Ricotti et al. 2006]. Conversely, perfect phase cocontinuity symmetry even for only two phases is only realizable in a very limited set of manners which are not isotropic [Burt and Korren 1996]. The general status of any partially bicontinuous two-phase structure is consequently an asymmetric bicontinuity.

(3) Both the phase continuity amount and the phase cocontinuity asymmetry are expected to be concentration-dependent for many materials, and this dependency is expected to obey many different law forms. In real materials, changes of phase concentration can be accompanied with changes in phase composition in addition to changes in phase arrangements, such that the phase properties do not remain fixed. In multiscale homogenization schemes, effective properties at inner levels can also change, which also corresponds to changes of the properties of assembled phases at the macroscopic level.

3. Layer-based approach of heterogeneous materials versus the aggregate-like description

Planar and linear cuts are, respectively, at the base of material reconstruction from 2D planar sections of the representative volume element (RVE) and from 1D-rays or lines traversing the RVE [Ramm and Katsevich 1996; Singh et al. 2008]. With regard to each direction $\boldsymbol{\omega}$ in space, any material either is a laminate structure whose layers are its planar heterogeneous sections normal to $\boldsymbol{\omega}$ or is a $\boldsymbol{\omega}$-directional fiber structure with the fibers being the material rays or lines in that $\boldsymbol{\omega}$ direction. While linear cuts necessarily alternate homogeneous subdomains of each phase, in planar sections (Figure 2) one phase can be multidirectionally macrocontinuous while all other ones are not. Sections consequently look like a patchwork of 2D subdomains within which one phase (at the most) is embedding all others in turn. Thus, 2D planar subdomains can be characterized by a continuous phase arranged into one infinite

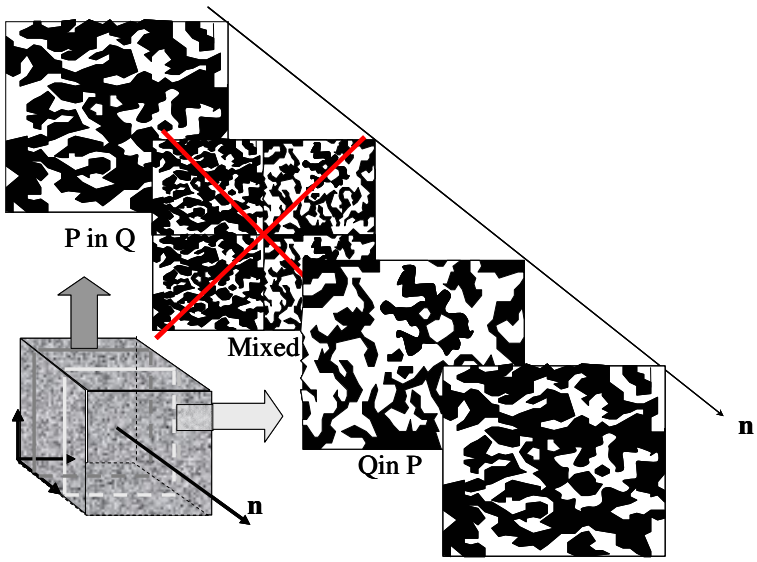

Figure 2. Typical planar sections of general two-phase materials.

cluster possibly having dead branches and being accompanied with finite clusters embedded in the other phase(s).

In planar sections of a two-phase material (p, q), the two phases p and q can only be locally arranged either as $p \subset q$ or as $q \subset p$ (also denoted as $p|q$ and $q|p$, respectively, in the following). For the sake of simplicity, we have ignored intermediate situations that can be resolved as smaller patchworks of these two same subdomains, and we have also disregarded the details of multiple inclusion levels such as $p \subset (q \subset p(\cdots))$, etc. This allows the description of any such macrohomogeneous material, with regard to any direction $\boldsymbol{\omega}$ and at the scale of a representative volume element, as a piling of parallel planes of $p|q$ and $q|p$ structures along $z(\boldsymbol{\omega})$, say as $\boldsymbol{\omega}$-oriented two-phase laminate structures. These planes of identical zero (or infinitesimal) thickness can be arranged into infinitely other sequences than the strictly alternated lamination. Assuming statistical homogeneity, the material phase concentrations are identically f_p and $f_q = 1 - f_p$ in each layer separately, for all directions $\boldsymbol{\omega}$. This is not saying that the material is an aggregate of laminate domains but that each material domain can be viewed from any direction $\boldsymbol{\omega}$ as a laminate structure, provided an appropriate description of the constitutive layers. One first property of importance for the following is that any $\boldsymbol{\omega}$-oriented laminate structure made of n different types of multiphase layers ensures the cocontinuity normally to $\boldsymbol{\omega}$ for all of the phases that are continuous in one layer type. When in a two-phase material (p, q) the $\boldsymbol{\omega}$-oriented layers have either a phase p or a phase q which is continuous, both phases p and q are cocontinuous normally to the direction $\boldsymbol{\omega}$. With regard to all other directions not normal to that $\boldsymbol{\omega}$, the continuity of each phase will depend on its through-section continuity, a crucial point to be closely examined latter on.

3.1. ***Effective elasticity properties of laminate structures in terms of platelet Green operators.*** In order to conveniently treat later on, for each $\boldsymbol{\omega}$ direction in $\mathbb{R}^3$, the two-phase material as such a laminate structure made of two types of sections $p|q$ and $q|p$, useful characteristics of laminate structures and of laminate layers (platelets) deserve to first be recalled.

Effective elasticity of laminates. There are various formulations to represent the effective properties of laminate structures, early calculated for example in [Postma 1955]. One is the hybrid procedure used in [El Omri et al. 2000] for modeling, in a plasticity context, polycrystalline structures as aggregates of laminate domains. Such a procedure is not to be used here, but this aggregate structure type will reappear in the following. The formulation more of concern here is the one which comes from the general homogenization framework for inclusion-reinforced matrices at the limit of infinitely flat and congruent spheroidal inclusions [Hill 1952; Zeller and Dederichs 1973; Walpole 1981]. Take a matrix of phase b, of moduli $\boldsymbol{C}_b$, reinforced with all congruent (shape V) ellipsoidal inclusions of phase ai, of moduli $\boldsymbol{C}_{ai}$, with concentrations c_{ai}, $i \in (1,\ n-1)$ and, according to a spatial distribution symmetry, homothetic to the shape V of all inclusions. The effective moduli read

$$\boldsymbol{C}^{*V}_{(a1,\dots,an-1)\subset b} = \boldsymbol{C}_b - \left(\left(\sum_{i=1}^{n-1} c_{ai}\left((\boldsymbol{C}_b - \boldsymbol{C}_{ai})^{-1} - \boldsymbol{t}^V_{C_b}\right)^{-1}\right)^{-1} + \boldsymbol{t}^V_{C_b}\right)^{-1} \tag{1}$$

Specializing to the case of platelets with $\boldsymbol{\omega}$-oriented normal ($V = P(\omega)$) amounts to substituting, in (1), the operator $\boldsymbol{t}^V_{C_b}$ with the operator $\boldsymbol{t}^{P(\omega)}_{C_b}$ that are respectively the modified strain Green operator integrals (strain Green operators or "GO$_\epsilon$" for short) for the inclusion V and for the platelet $P(\omega)$, in an infinite matrix of moduli $\boldsymbol{C}_b$. It is a key property of laminate structures that any one of the n layer types can be selected as the "matrix" without changing the result. For a two-phase material (a, b) of the laminate type, setting $\boldsymbol{\Delta C}_{b|a} = \boldsymbol{C}_b - \boldsymbol{C}_a = -\boldsymbol{\Delta C}_{a|b}$, the following equation results:

$$\boldsymbol{C}^{*P(\omega)}_{a\subset b} = \boldsymbol{C}_b - c_a\left((\boldsymbol{\Delta C}_{b|a})^{-1} - c_b\boldsymbol{t}^{P(\omega)}_{C_b}\right)^{-1} = \boldsymbol{C}^{*P(\omega)}_{b\subset a} = \boldsymbol{C}_a - c_b\left((\boldsymbol{\Delta C}_{a|b})^{-1} - c_a\boldsymbol{t}^{P(\omega)}_{C_a}\right)^{-1} \tag{2}$$

and the proof of the equality $\boldsymbol{C}^{*P(\omega)}_{a\subset b} = \boldsymbol{C}^{*P(\omega)}_{b\subset a} = \boldsymbol{C}^{*P(\omega)}_{a,b}$ (which only holds for platelet-like inclusions) is recalled in Appendix A. For $\boldsymbol{\omega}$-oriented fibers $F(\omega)$, also a specific case of interest later on, one obtains

$$\boldsymbol{C}^{*F(\omega)}_{a\subset b} = \boldsymbol{C}_b - c_a\left((\boldsymbol{\Delta C}_{b|a})^{-1} - c_b\boldsymbol{t}^{F(\omega)}_{C_b}\right)^{-1} \neq \boldsymbol{C}^{*F(\omega)}_{b\subset a} = \boldsymbol{C}_a - c_b\left((\boldsymbol{\Delta C}_{a|b})^{-1} - c_a\boldsymbol{t}^{F(\omega)}_{C_a}\right)^{-1} \tag{3}$$

In (3), the operator $\boldsymbol{t}^{F(\omega)}_{C_b}$ is the GO$_\epsilon$ for the fiber $F(\omega)$ in an infinite matrix of moduli $\boldsymbol{C}_b$. When $\boldsymbol{t}^V_{C_b}$ is used instead of $\boldsymbol{t}^{F(\omega)}_{C_b}$ (resp. $\boldsymbol{C}_a$), (3) gives the two specializations of (1) for a two-phase material which are the HS (Hashin–Shtrikman) bounds [1963] for all the spatial distributions of the phases a and b characterized by the shape V.

Equations (2)–(3), which hold for moduli tensors $\boldsymbol{C}$, have corresponding forms for the related compliance tensors $\boldsymbol{S} = \boldsymbol{C}^{-1}$, when the appropriate modified stress Green operator integral (stress Green operators or GO$_\sigma$ for short) $\boldsymbol{t}'^V_{S_b}$ is substituted with $\boldsymbol{t}^V_{C_b}$.

Table 1 collects the nonzero terms of these strain Green operators $\boldsymbol{t}^V_{C_b}$ and stress Green operators $\boldsymbol{t}'^V_{S_b}$ for the sphere, the x_3-oriented platelet and the x_3-oriented fiber. They depend on the two constants

$$B = \frac{1}{\mu} \quad \text{and} \quad A = \frac{-B}{2(1-\nu)}$$

for the isotropic elasticity of a matrix phase of shear modulus μ and Poisson coefficient ν.

For isotropic properties that are represented by rank-two tensors, as dielectric ones [Helsing 1993; Fan 1995; Kanaun 2003], there is no term A and the term B acts as the inverse of the dielectric constant. The relationships between these operators, for any ellipsoidal inclusion type V [Zeller and Dederichs 1973]

	t_{iiii}	t_{1122}	t_{ii33}	t_{3333}	t_{i3i3}	t_{1212}
sphere	$\frac{3A+5B}{15}$	$\frac{A}{15}$	$\frac{A}{15}$	$\frac{3A+5B}{15}$	$\frac{2A+5B}{30}$	$\frac{2A+5B}{30}$
x_3-platelet	0	0	0	$A+B=\frac{1}{\lambda+2\mu}$	$\frac{B}{4}=\frac{1}{4\mu}$	0
x_3-cylinder	$\frac{3A+4B}{8}$	$\frac{A}{8}$	0	0	$\frac{B}{8}$	$\frac{A+2B}{8}$

	t'_{iiii}	t'_{1122}	t'_{ii33}	t'_{3333}	t'_{i3i3}	t'_{1212}
sphere	$-\frac{32A}{15B^2}$	$-\frac{2(12A+5B)}{15B^2}$	$-\frac{2(12A+5B)}{15B^2}$	$-\frac{32A}{15B^2}$	$\frac{5B-4A}{15B^2}$	$\frac{5B-4A}{15B^2}$
x_3-platelet	$-\frac{4A}{B^2}=\frac{2\mu}{1-\nu}$	$-\frac{2(2A+B)}{B^2}$	0	0	0	$\frac{1}{B}=\mu$
x_3-cylinder	$-\frac{3A}{2B^2}$	$-\frac{A}{2B^2}$	$-\frac{A}{B^2}$	$-\frac{4A}{B^2}$	$\frac{1}{2B}$	$-\frac{A}{2B^2}$

Table 1. Strain Green operators $\boldsymbol{t}$ (top table) and stress Green operators $\boldsymbol{t}'$ (bottom table) for a sphere, an x_3-platelet and an x_3-cylinder in isotropic media ($i=1,2$).

with $\boldsymbol{C}_b=(\boldsymbol{S}_b)^{-1}$, are described by

$$\overline{\boldsymbol{t}'^{V}_{S_b}}=\boldsymbol{C}_b-\boldsymbol{C}_b:\overline{\boldsymbol{t}^{V}_{C_b}}:\boldsymbol{C}_b \quad \text{and} \quad \overline{\boldsymbol{t}^{V}_{C_b}}=\boldsymbol{S}_b-\boldsymbol{S}_b:\overline{\boldsymbol{t}'^{V}_{S_b}}:\boldsymbol{S}_b \tag{4}$$

A well known property of platelet operators that are related to a same normal direction $\boldsymbol{\omega}$ is their direct relation to the stress and strain jumps on both sides of a phase interface with normal $\boldsymbol{\omega}$ [Walpole 1978; 1981]. Less known is that any GO_ϵ (resp. GO_σ) operator related to an ellipsoidal shape of inclusion or distribution can be decomposed into a weighted average of GO_ϵ (resp. GO_σ) platelet operators over all directions $\boldsymbol{\omega}$ in space, according to its polar or spectral decomposition given by the Radon inversion formula [Gel'fand et al. 1966; Ramm and Katsevich 1996], that is,

$$\boldsymbol{t}^{V}_{C}=\int_\Omega \boldsymbol{\psi}^{V}(\omega)\boldsymbol{t}^{P(\omega)}_{C}\,\mathrm{d}\omega \quad ; \quad \boldsymbol{t}'^{V}_{S}=\int_\Omega \boldsymbol{\psi}^{V}(\omega)\boldsymbol{t}'^{P(\omega)}_{S}\,\mathrm{d}\omega \tag{5}$$

In the isotropic (spherical) case, the weight function of this decomposition ($\boldsymbol{\psi}^{V}(\omega)\geq 0$, $\int_\Omega \boldsymbol{\psi}^{V}(\omega)\,\mathrm{d}\omega=1$) uniformly equals $\boldsymbol{\psi}^{\mathrm{Sph}}(\omega)=(4\pi)^{-1}$, while for a platelet of $\boldsymbol{\omega}_0$ normal it reduces to a Dirac function if $\boldsymbol{\psi}^{P(\omega 0)}(\omega)=\delta(\omega-\omega 0)$. For $\boldsymbol{\omega}_0$ -oriented cylindrical fibers, the weight function $\boldsymbol{\psi}^{F(\omega 0)}(\omega)$ equals $(2\pi)^{-1}$ for all directions normal to the fiber axis $\boldsymbol{\omega}_0$ and is zero otherwise. These Radon forms of Green operators have been discussed in [Franciosi and Lormand 2004; Franciosi 2005; 2010] for inclusions of various shapes and inclusion patterns of various spatial arrangements.

Further properties of platelet Green operators. Simple mathematical manipulations allow the demonstration (Appendix A) that for two-phase laminates in relative phase proportions c_a, c_b, the effective moduli take the symmetric form that appears in [Cherkaev 2000] in a less explicit manner:

$$\boldsymbol{C}^{*P(\omega)}_{a,b}=\langle \boldsymbol{C}\rangle-c_a c_b\boldsymbol{\Delta C}_{b|a}:\boldsymbol{t}^{P(\omega)}_{\{\boldsymbol{C}\}}:\boldsymbol{\Delta C}_{b|a} \tag{6}$$

with $\langle \boldsymbol{C} \rangle = c_a \boldsymbol{C}_a + c_b \boldsymbol{C}_b$ and $\{\boldsymbol{C}\} = c_b \boldsymbol{C}_a + c_a \boldsymbol{C}_b$ being respectively the Voigt (V) moduli tensor for the material $[a, b]$ and the one for its "complementary material" $]a, b[$ defined by an interchange of the phase proportions, say c_a of phase b and c_b of phase a. The dual expressions to (2) and (3) for the effective compliances $\boldsymbol{S}^{*V}_{a,b} = (\boldsymbol{C}^{*V}_{a,b})^{-1}$ read as follows (Appendix B), with $\boldsymbol{\Delta S}_{a|b} = \boldsymbol{S}_a - \boldsymbol{S}_b$ and with the appropriate GO_σ operator $\boldsymbol{t'}^V_{Sb} = \boldsymbol{t'}^{P(\omega)}_{Sb}$ for laminates and $\boldsymbol{t'}^V_{Sb} = \boldsymbol{t'}^{F(\omega)}_{Sb}$ for fibers:

$$\boldsymbol{S}^{*V}_{a\subset b} = \boldsymbol{S}_b - c_a \big((\boldsymbol{\Delta S}_{b|a})^{-1} - c_b \boldsymbol{t'}^V_{s_b} \big)^{-1} \tag{7}$$

Equation (7) also uses the equations (4), which connect $(\boldsymbol{\Delta S}_{b|a})^{-1}$ to $(\boldsymbol{\Delta C}_{b|a})^{-1}$ as they connect $\overline{\boldsymbol{t'}^V_{Sb}}$ to $\overline{\boldsymbol{t}^V_{Cb}}$, say

$$(\boldsymbol{\Delta S}_{b|a})^{-1} = \boldsymbol{C}_b - \boldsymbol{C}_b : (\boldsymbol{\Delta C}_{b|a})^{-1} : \boldsymbol{C}_b, \quad (\boldsymbol{\Delta C}_{b|a})^{-1} = \boldsymbol{S}_b - \boldsymbol{S}_b : (\boldsymbol{\Delta S}_{b|a})^{-1} : \boldsymbol{S}_b \tag{8}$$

The particular symmetric form reported in (6) for (2) which gives the effective moduli tensor of a two-phase laminate structure has its equivalent form for the dual effective compliance tensor. Noticing that $\langle \boldsymbol{S} \rangle \neq \langle \boldsymbol{C} \rangle^{-1}$ and $\{\boldsymbol{S}\} = c_b \boldsymbol{S}_a + c_a \boldsymbol{S}_b \neq \{\boldsymbol{C}\}^{-1}$, it reads

$$\boldsymbol{S}^{*P(\omega)}_{a,b} = \langle \boldsymbol{S} \rangle - c_a c_b \boldsymbol{\Delta S}_{b|a} : \boldsymbol{t'}^{P(\omega)}_{\{\boldsymbol{S}\}} : \boldsymbol{\Delta S}_{b|a} \tag{9}$$

with the "stress" Green operator referring to the Reuss (R) compliance tensor $\{\boldsymbol{S}\}$ of the complementary composite $]a, b[$, while $\langle \boldsymbol{S} \rangle = c_a \boldsymbol{S}_a + c_b \boldsymbol{S}_b$ is the one of the material $[a, b]$. From the many relations between $\langle \boldsymbol{C} \rangle$, $\langle \boldsymbol{S} \rangle$, $\{\boldsymbol{C}\}$ and $\{\boldsymbol{S}\}$[3], one has in particular the equivalences

$$\boldsymbol{\Delta C}_{b|a} = \frac{\{\boldsymbol{C}\} - \boldsymbol{C}_a}{c_a} = -\frac{\{\boldsymbol{C}\} - \boldsymbol{C}_b}{c_b}; \quad \boldsymbol{\Delta S}_{b|a} = \frac{\{\boldsymbol{S}\} - \boldsymbol{S}_a}{c_a} = -\frac{\{\boldsymbol{S}\} - \boldsymbol{S}_b}{c_b} \tag{10}$$

Using (10) in (6) and (9) yields these remarkable estimate forms for two-phase laminates:

$$\boldsymbol{C}^{*P(\omega)}_{a,b} = \langle \boldsymbol{C} \rangle + (\{\boldsymbol{C}\} - \boldsymbol{C}_a) : \boldsymbol{t}^{P(\omega)}_{\{\boldsymbol{C}\}} : (\{\boldsymbol{C}\} - \boldsymbol{C}_b), \tag{11a}$$

$$\boldsymbol{S}^{*P(\omega)}_{a,b} = \langle \boldsymbol{S} \rangle + (\{\boldsymbol{S}\} - \boldsymbol{S}_a) : \boldsymbol{t'}^{P(\omega)}_{\{\boldsymbol{S}\}} : (\{\boldsymbol{S}\} - \boldsymbol{S}_b). \tag{11b}$$

Not only do Equations (6), (9) and (11a), (11b) incidentally provide new relations between the Green operators of $\boldsymbol{\omega}$-oriented platelets associated with a pair of complementary materials ($[a, b]$, $]a, b[$), but they also essentially reveal the role, to be examined later on, of the two-phase complementary composite $]a, b[$ as a reference medium. The moduli estimates for n types of layers are obtained by recurrence, adding the n-th layer type to the $(n-1)$-laminate previously assembled by adding the $(n-1)$-st layer type to the $(n-2)$ previously assembled ones, and so on. A symmetric form is obtained by averaging over all possible choices for the order or the layered phases. This symmetric form generalizing (11) to n phases is to be presented in a separate work.

3.2. ***Isotropic platelet systems (IPS) for bicontinuous two-phase materials.*** One of the first proposed effective moduli estimates for bicontinuous two-phase materials refers to laminate structures. It is the one which comes from the isotropic platelet system (IPS) introduced in [Christensen 1979a; 1979b]. The IPS estimate is defined as the isotropic averaging of the effective moduli tensor for the $\boldsymbol{\omega}$-oriented

[3] Such as $\langle \boldsymbol{C} \rangle : \boldsymbol{\Delta S}_{b|a} = \boldsymbol{\Delta C}_{a|b} : \{\boldsymbol{S}\}$ or $\langle \boldsymbol{C} \rangle : \langle \boldsymbol{S} \rangle = \{\boldsymbol{C}\} : \{\boldsymbol{S}\} = \boldsymbol{I} - f_a f_b \boldsymbol{\Delta C}_{b|a} : \boldsymbol{\Delta S}_{b|a}$.

	$iiii(0,0)$	$3333(0,0)$	$1122(0,0)$	$ii33(0,0)$	$1212(0,0)$	$i3i3(0,0)$
$\overline{jjjj(\theta,\phi)}$	$\frac{8}{15}$	$\frac{3}{15}$	0	$\frac{4}{15}$	0	$\frac{8}{15}$
$\overline{jjkk(\theta,\phi)}$	$\frac{1}{15}$	$\frac{1}{15}$	$\frac{5}{15}$	$\frac{8}{15}$	0	$-\frac{4}{15}$
$\overline{jkjk(\theta,\phi)}$	$\frac{1}{15}$	$\frac{1}{15}$	0	$-\frac{2}{15}$	$\frac{5}{15}$	$\frac{6}{15}$

Table 2. Coefficients giving the isotropic average of axially symmetric operators ($i = 1, 2$; $j, k = 1, 2, 3$).

laminate systems, from (2), (6) or (11a):

$$\boldsymbol{C}^{*\mathrm{IPS}}_{a,b} = (4\pi)^{-1} \iint_{\theta,\phi} \boldsymbol{C}^{*P(\theta,\phi)}_{a,b}(\theta,\phi)\sin\theta\,\mathrm{d}\theta\,\mathrm{d}\phi \tag{12}$$

where one has, by rotation of matrix $[W]$, the relations $(\boldsymbol{C}^{*P(\theta,\phi)}_{a,b})_{ijkl} = W_{ip}W_{jq}W_{kr}W_{ls}(\boldsymbol{C}^{*P(0,0)}_{a,b})_{pqrs}$. The IPS, as introduced, was said by the author as "implying intersecting platelets of some kind" and "suggestive of morphology known as interpenetrating networks" of (two) phases. This IPS results from performing a geometric averaging process previously applied to isotropic fiber systems (IFSs) in [Christensen and Waals 1972], fiber systems which will be examined later on. With considering layers of the two constitutive phases (p, q) of the material, this IPS estimate is expected to ensure some isotropic phase cocontinuity; because, as underlined previously, for each $\boldsymbol{\omega}$ direction the layered structure ensures the phase cocontinuity normally to $\boldsymbol{\omega}$ and because $\boldsymbol{\omega}$ is taken to span the whole space. However, no material strictly having that type of phase organization is realizable: if it happens that normally to one direction $\boldsymbol{\omega}$ the two phases (p, q) exhibit a laminate-like organization, there is no direction $\boldsymbol{\omega}' \neq \pm\boldsymbol{\omega}$ possibly exhibiting the same organization simultaneously. Aware of this, Christensen imaged the arrangement of this IPS structure as an isotropic aggregate of $\boldsymbol{\omega}$-oriented laminate domains, but this does not satisfactorily depict an interpenetrating network of two phases, and the effective properties of such an aggregate of laminate domains are not properly estimated by (12). An aggregate of laminate domains is more convenient to describe planar slip in grains of polycrystals, as used by [El Omri et al. 2000] for plasticity modeling.[4] Conversely, this slip description illustrates what kind of trans-granular continuity one can expect between the layers of a same phase which are randomly oriented from grain to grain: it is no more than the possible slip continuity between neighboring grains. A better estimate for the elasticity moduli of an aggregate of laminate domains is the one obtained from the SC approximation

$$\boldsymbol{C}^* = \boldsymbol{C}^* - \left(\left(\frac{1}{4\pi}\int_\Omega \left((\boldsymbol{C}^* - \boldsymbol{C}^P\omega)^{-1} - \boldsymbol{t}^{\mathrm{Sph}}_{\boldsymbol{C}^*}\right)^{-1}\mathrm{d}\omega\right)^{-1} + \boldsymbol{t}^{\mathrm{Sph}}_{\boldsymbol{C}^*}\right)^{-1}, \tag{13}$$

where the tensors $\boldsymbol{C}^P\omega$ are the moduli tensors for the ω-oriented laminated grains, given in (6) and (11a). The IPS estimate from (12) is definitely different from the one of (13), to be denoted ISCP in further comparisons. As is easily checked for the shear modulus in the case of two incompressible phases (combine (6) and (13) with using Table 2), when the phase contrast becomes infinite (taking one phase as void-like), this ISCP estimate goes to zero as the Reuss (R) and the HS(−) lower bounds, although in

[4] See also [Franciosi and Berbenni 2007; 2008] for laminate modeling of plastic slip in polycrystals.

a much slower manner. An interpretation is that even if large and intricate clusters of both phases exist, due to trans-granular chord connections between layers of a same phase, the probability of finding an infinite homogeneous path from grain to grain goes to zero with increasing the grain number to cross, and infinite clusters of each phase therefore have vanishingly small contributions. However, the quite high stiffness of the ISCP estimate from (13) makes it probably convenient for intricate mixtures of long tortuous fibers, as in cotton-like tangled or muddled assemblages of two fiber types, for example.

It is clear from all what precedes that the morphology types represented by (12) have to be seen as having the properties of an IPS more in a statistical way than effectively, owing to the impossible IPS topology as strictly defined. It is noteworthy at this stage that (12) has a likely interpretation in terms of a Radon inversion formula, as (5) has for the stress and strain Green operators: (12) can be understood as some spectral decomposition over a set of elementary effective moduli tensors, each representative of a typical planar connectivity property for layers of the materials of concern.

This interpretation would result from particular assumptions on the effective properties at the level of the material sections as exemplified in [Errabii et al. 2007]. Consistently with this view-point, the Christensen interpretation becomes acceptable provided the essential modification we here use that the involved representative "phases" a and b for the layer types are not the constitutive phases (p, q) of the material but are the homogeneous materials "equivalent" to the two types of its $p|q$ and $q|p$ heterogeneous sections, in a way which has to be appropriately defined, as examined in the following.The isotropic arithmetic average from (12) of an operator $\boldsymbol{C}^{*0}$ that corresponds to a structure with an x_3-oriented symmetry yields an isotropic tensor with eigenvalues which can be simply explicated using the relations

$$\begin{aligned} \boldsymbol{C}^{*\mathrm{iso}}_{ijij} &= \tfrac{1}{15}(\boldsymbol{C}^{*0}_{3333} + \boldsymbol{C}^{*0}_{iiii} - 2\boldsymbol{C}^{*0}_{ii33}) + \tfrac{1}{15}(6\boldsymbol{C}^{*0}_{i3i3} + 5\boldsymbol{C}^{*0}_{1212}), \\ \boldsymbol{C}^{*\mathrm{iso}}_{iiii} + 2\boldsymbol{C}^{*\mathrm{iso}}_{iijj} &= \tfrac{5}{15}(\boldsymbol{C}^{*0}_{3333} + 2\boldsymbol{C}^{*0}_{iiii} + 4\boldsymbol{C}^{*0}_{ii33} + 2\boldsymbol{C}^{*0}_{1122}). \end{aligned} \tag{14}$$

In (14) the coefficients are the isotropy coefficients of Table 2, obtained by solving simple trigonometric integrals. The IPS estimate from (12) results from using, as C^{*0} in (14), the laminate effective moduli given by (2) with the GO_ϵ of the x_3-oriented platelet given in Table 1, top. Now, a theoretical form of interest for the effective IPS properties can be obtained from (11a) as

$$\begin{aligned} C^{*\mathrm{IPS}}_{a,b} &= \int_\Omega \frac{C^{*^P}(\omega)}{4\pi}\,\mathrm{d}\omega = \langle \boldsymbol{C}\rangle - c_a c_b \boldsymbol{\Delta C}_{b|a} : \left(\int_\Omega \frac{t^P_{\{C\}}(\omega)}{4\pi}\,\mathrm{d}\omega \right) : \boldsymbol{\Delta C}_{b|a} \\ &= \langle \boldsymbol{C}\rangle - c_a c_b \boldsymbol{\Delta C}_{b|a} : \boldsymbol{t}^{\mathrm{Sph}}_{\{\boldsymbol{C}\}} : \boldsymbol{\Delta C}_{b|a} = \langle \boldsymbol{C}\rangle + (\{\boldsymbol{C}\} - \boldsymbol{C}_a) : \boldsymbol{t}^{\mathrm{Sph}}_{\{\boldsymbol{C}\}} : (\{\boldsymbol{C}\} - \boldsymbol{C}_b). \end{aligned} \tag{15}$$

The important result expressed by (15) is the symmetric dependence of the IPS on a single operator. This point will be of use in the sequel. In (15), the operator $\boldsymbol{t}^{\mathrm{Sph}}_{\{\boldsymbol{C}\}}$ is the GO_ϵ for a spherical inclusion embedded in a matrix of moduli $\{\boldsymbol{C}\}$, given by its polar (Radon) decomposition in (5), where a and b are the effective properties of the representative planar sections which will be estimated in the following. In terms of compliances, although $\boldsymbol{S}^{*P(\omega)}_{a,b} = (\boldsymbol{C}^{*P(\omega)}_{a,b})^{-1}$, one has, in general,

$$\boldsymbol{S}^{*\mathrm{IPS}}_{a,b} = (4\pi)^{-1} \int_\Omega \boldsymbol{S}^{*^P}(\omega)\,\mathrm{d}\omega \neq (\boldsymbol{C}^{*\mathrm{IPS}}_{a,b})^{-1}.$$

This dual average (to be examined in a separate paper) corresponds to dual stress conditions that are not expected to be fulfilled by the phases of cocontinuous structures.

3.3. *Link and differences between the IPS and the isotropic self-consistent (ISC) estimates.*

Compared IPS and ISC estimates in terms of reference medium. The self-consistent (SC) approximation for aggregates of congruent grains is considered to account well for a phase continuity inversion in two-phase materials when the dense/dilute concentrations are inverted and for an intermediate domain of bicontinuity. When the grains are as flat as layers of a laminate structure, the SC approximation is also given by (3) because the HS(+/−) bounds coincide in this case. The calculation of the SC approximation is recalled in Appendix B. As the IPS estimates, various isotropic SC (ISC) approximations can be obtained with considering the various sets of reference phases $(a, b, \dots)$ that result from some preliminary homogenization level(s) on the constitutive phases $(p, q, \dots)$. Remarkably, it is shown in the Appendix C that for two-phase materials and in the isotropic case, the ISC estimate can be also written under a form similar to the IPS estimate in (15), say

$$\boldsymbol{C}^{*\mathrm{ISC}}_{a,b} = \langle \boldsymbol{C} \rangle + (\boldsymbol{C}^{*\mathrm{ISC}}_{a,b} - \boldsymbol{C}_a) : \boldsymbol{t}^{\mathrm{Sph}}_{\boldsymbol{C}^{*\mathrm{ISC}}_{a,b}} : (\boldsymbol{C}^{*\mathrm{ISC}}_{a,b} - \boldsymbol{C}_b) = (\boldsymbol{S}^{*\mathrm{ISC}}_{a,b})^{-1} \tag{16}$$

Equation (16), as a particular form of the ISC approximation for two-phase material not found in the literature to the authors knowledge, provides when comparing with the IPS estimate in (15) new insights of interest with regard to phase cocontinuity representations. For any phase number $n-1$, the generally implicit ISC estimate is fast calculated iteratively from an explicit one such as (1), using an arbitrary initial admissible matrix as the n-th phase. For two phases, one verifies that it can be also fast iterated from the IPS explicit estimate of (15) that converges to the form of (16)[5]. The new insight from comparing (15) and (16) can be put as follows: the SC approximation treats the two-phase material as a three-phase structure where a matrix of infinitesimal volume fraction (the reference medium) embeds the two types of grains. While in the ISC approximation the reference medium (the infinitesimal matrix) is the homogeneous equivalent material itself, in the IPS estimate, (15) identifies the third phase reference matrix to be a Voigt-type (V) structure of the complementary composite $]a, b[$. A comparison of (15) with (16) conversely provides for the IPS estimate the form which enters the general expression reported in (1) as

$$\boldsymbol{C}^{*\mathrm{IPS}}_{(a,b)} = \{\boldsymbol{C}\} - \Big(\Big(c_a \big((\{\boldsymbol{C}\} - \boldsymbol{C}_a)^{-1} - \boldsymbol{t}^{\mathrm{Sph}}_{\{\boldsymbol{C}\}} \big)^{-1} + c_b \big((\{\boldsymbol{C}\} - \boldsymbol{C}_b)^{-1} - \boldsymbol{t}^{\mathrm{Sph}}_{\{\boldsymbol{C}\}} \big)^{-1} \Big)^{-1} + \boldsymbol{t}^{\mathrm{Sph}}_{\{\boldsymbol{C}\}} \Big)^{-1} \tag{15}$$

The similarity established here allows a sound understanding of why the IPS estimate has a strong legitimacy to represent structures having (no matter how) a total cocontinuity of the two phases over the whole range of phase concentration: the reference structure of the IPS is shown to be an aggregate of two phases embedded in an infinitesimal third phase layer of the complementary composite $]a, b[$ arranged into a parallel-like (Voigt-like) mixture of the two phases, where the dilute phase of the bulk is dominant. The consequence is that, considering a highly dilute phase a (resp. b) in the bulk, isolated grains of phase a infinitely far from each other remain connected by the infinitely extended interfacial links in the layer where phase a (resp. b) highly dominates. Conversely, highly concentrated grains of phase b (resp. a) only need a little quantity of phase b (resp. a) in the matrix layer for helping being interconnected.

[5]The same holds for $n > 2$ using the appropriate forms for the IPS- and the ISC-related estimates that we have obtained and are not discussed here

Compared IPS and ISC estimates in terms of phase cocontinuity requests. One second important request for an IPS to be consistent with the cocontinuity of the constitutive phases is for the through-section continuity to be at least partially fulfilled by both phases. For example, planar sections of pure phase p or q are inconsistent with through-section cocontinuity. Planar sections where the phases p and q are arranged in Reuss-type (R) or in HS-type manners are also incompatible with through-section bicontinuity, and so on.

In comparison, making use of an ISC approximation to describe a bicontinuous two-phase medium (p, q) as an aggregate made of grains a and b, requires these grains to be, at least partially, bicontinuous for a possible phase bicontinuity in all proportions though the grain boundaries. Grains of pure phase $(a = p, b = q)$ are consistent with bicontinuity only at comparable proportions of phases (a, b). Grains of Reuss-type effective properties are not relevant at all concentrations because they yield no continuity when the Reuss-type grains dominate. Grain mixtures of HS$(+/-)$ types are consistent with only partial bicontinuity because of the embedded phase part, etc.

In consequence, in order to make the phase cocontinuity possible through material layers in a laminate description or through grain boundaries in an aggregate description, at any phase concentration, we have referred to fiber systems to describe the effective properties of representative layers and grains.

4. The description of the phase cocontinuity from fiber systems

We consider two-phase isotropic materials (p, q) of the reinforced-matrix type, with a part of the p (resp. q) isotropically oriented inclusions being taken as infinite fibers. The presence of such infinite fibers in these "reference reinforced matrices" ensures a cocontinuity of the two (matrix and fiber) phases. Continuous orientation sets of infinite fibers are called fiber systems in general, as illustrated on each side of Figure 3, and isotropic fiber systems (IFSs) in the particular isotropic situations. Assembling

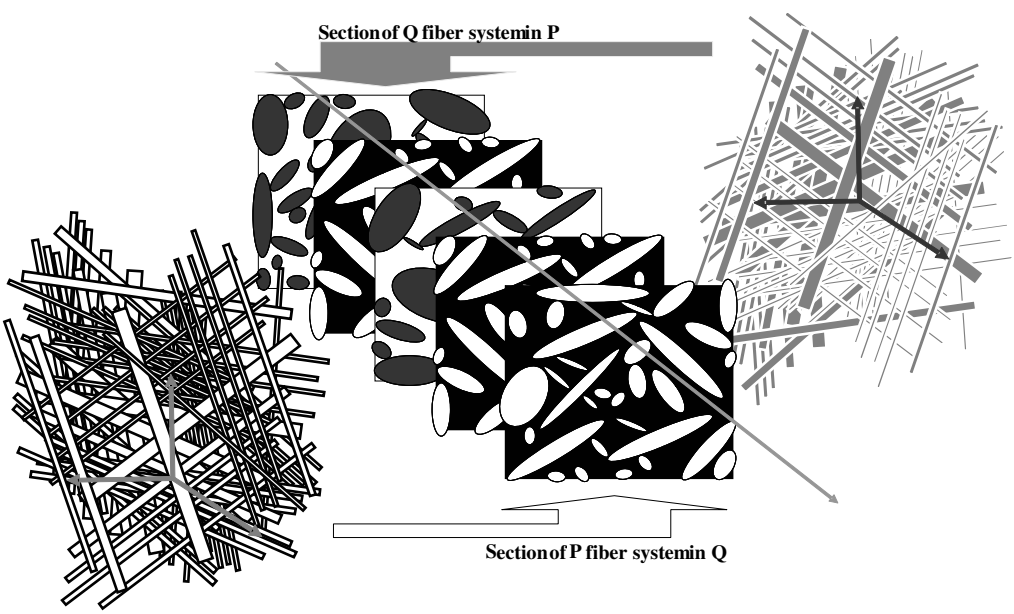

Figure 3. Typical planar sections of isotropic fiber systems.

aggregates of grains of types a and b made of such phase cocontinuous materials ($q \subset p$ for a and $p \subset q$ for b), also ensure long range cocontinuity of the two phases p and q. Now, planar sections of such IFSs are, as drawn in the middle of Figure 3, assemblages of elliptical domains possibly exhibiting all sizes, aspect ratios and orientations. In reconstructed laminations from piling the two types $a(q \subset p)$ and $b(p \subset q)$ of such sections, both phases p and q are possibly continuous between neighboring layers similarly described. Thanks to contacts between surfaces of a same phase p (resp. q), these phase connections across layers a and b allow realizations of continuous arrangements of the phases p and q a priori along all through-layer directions. Consequently, taking sections of IFSs as reference layers in a layer-based homogenization approach of the IPS type or taking grains of IFSs as reference grains in an aggregate approach of ISC type are two descriptions consistent with the possible cocontinuity of the phases throughout the material volume. The so-obtained two estimates from this two-scale procedure will be denoted IPS-IFS and ISC-IFS, respectively.

From their distinct definition or construction, a slight difference distinguishes these two structures and consequently their related estimates. This difference, as made precise later, concerns the limit situations when going either towards null or total phase cocontinuity. Towards null cocontinuity, the difference rests in the amount of residual phase cocontinuity, vanishing to zero in both descriptions but not being rigorously prohibited by construction. A larger residue probably is likely for the layer-based approach. Conversely, towards the total cocontinuity, reintroducing dead branches in the sample spanning clusters of each phase is not rigorously impossible by the structure constructions, either when piling layers of when assembling grains.

Isotropic fiber systems in real materials with two homogeneous phases are realizable in a concentration range that depends on the considered number of fiber directions to realize isotropy. Dendievel et al. [2002] have shown the realizability of fiber arrangements having dodecahedral symmetry (Figure 4a) and it has been established in [Franciosi 2005] how and why finite sets of directions belonging to the dodecahedral-icosahedral symmetry class yield isotropic mean Green operators and consequently isotropic effective properties. Such patterns can be taken as representative of elementary volumes in real fiber systems, as with those exemplified in the middle and right portions of Figure 4. Unavoidable fiber waviness (tortuousness) to reach high fiber concentrations does not much affect the topology of planar sections. The comparison of Figure 3 with Figure 2 shows that the main missing topological properties in our idealized

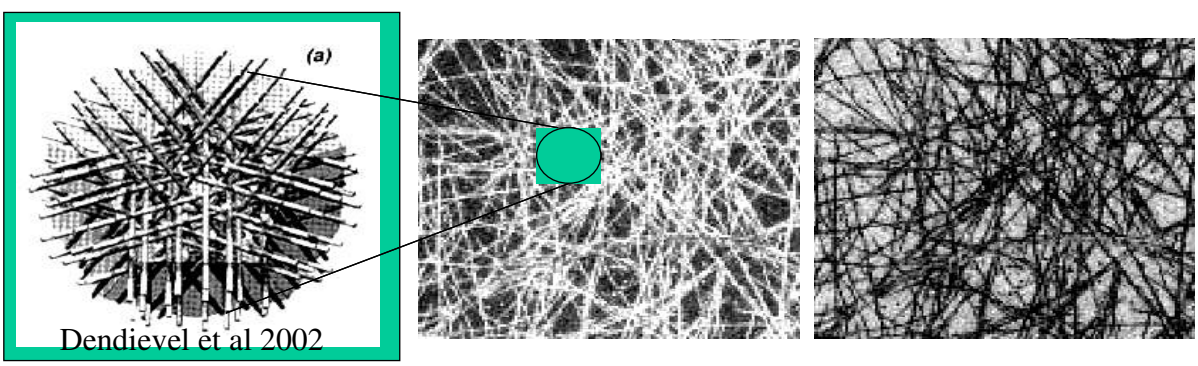

Figure 4. Left: isotropic fiber system built by Dendievel et al. [2002]. Middle and right: real dual 3D isotropic fiber structures.

section description (in addition to the disregarded $p \subset (q \subset p(\cdots))$ multiply embedded patterns) are this nonzero tortuousness of the fibers and the nonconvexity of the 2D bounded domains in the planar sections of real materials. However, we consider that neither one is essential in defining which of the two phases is macrocontinuous in sections. Still, for the sake of simplicity, aside from the infinite cluster of each phase represented by the infinite fibers as assembled, the possibility of finite clusters and of dead branches has been globally accounted for by a volume fraction of spherical (thus embedded) domains, owing to the overall isotropy assumption[6].

4.1. *Effective moduli for generalized IFSs.*

Isotropic fiber systems. The effective moduli for such IFS structures are obtained, following [Christensen 1979a], by "averaging an assigned strain state" over all the positions in space of a directional fiber system, as done for the effective moduli of IPS structures from a laminate. The average over the stresses that results from imposing the same strain in all possible directions with regard to a directional fiber system $\boldsymbol{\omega}$ is taken as equivalent to the stresses obtained when imposing the strain on a material reinforced with an isotropic orientation of fibers. Using (3) with $(a, b) = (p, q)$ and $c_a = f_p$, $c_b = f_q$ as the nominal phase concentrations, the resulting effective moduli for the IFSs upon averaging on $\boldsymbol{\omega} = (\theta, \phi)$ over $\mathbb{R}^3$ read

$$\boldsymbol{C}^{*\mathrm{IFS}}_{p\subset q} = \int_\Omega \frac{\boldsymbol{C}^{*F}_{p\subset q}(\omega)}{4\pi}\,\mathrm{d}\omega, \quad \boldsymbol{C}^{*\mathrm{IFS}}_{q\subset p} = \int_\Omega \frac{\boldsymbol{C}^{*F}_{q\subset p}(\omega)}{4\pi}\,\mathrm{d}\omega. \tag{17}$$

The explicit forms of these IFS moduli result from using the coefficients of Table 2 with the effective moduli of the x_3-oriented fiber systems from (3), for which the GO_ϵ of the x_3-cylinder given in Table 1, top, is introduced. The IFSs are the isotropic superposition of directional $\boldsymbol{\omega}$-oriented fiber systems whose effective moduli $\boldsymbol{C}^{*F(\omega)}_{p\subset q}$ and $\boldsymbol{C}^{*F(\omega)}_{q\subset p}$ are the HS bounds for transversally isotropic material of the ω symmetry axis. As in the platelet case, the average over all $\boldsymbol{\omega}$ directions does not fulfill the inversion property, say

$$\boldsymbol{S}^{*\mathrm{IFS}}_{p\subset q} = \int_\Omega \frac{\boldsymbol{S}*^{F}_{p\subset q}(\omega)}{4\pi}\,\mathrm{d}\omega \neq \big(\boldsymbol{C}^{*\mathrm{IFS}}_{p\subset q}\big)^{-1},$$

although $\boldsymbol{S}^{*F(\omega)}_{p\subset q} = \big(\boldsymbol{C}^{*F(\omega)}_{p\subset q}\big)^{-1}$ (and likewise with $q \subset p$) and the compliance averaging from the request of stress compatibility between the fibers and the entire RVE does not correspond to a characteristic of cocontinuous structures.

Generalized isotropic fiber systems. The generalization of the IFS that is introduced allows the construction of partially (total to null) cocontinuous phase arrangements. We introduce the fraction ϕ_p of the phase p consisting of infinite fibers included in the reference reinforced matrix q, and conversely ϕ_q for fibers q in matrix p. If phase p is included with a nominal concentration f_p, then the fraction of infinite fibers p is $\phi_p f_p$ and it represents the fraction of phase p that belongs to an infinite (sample spanning) cluster; this is the fraction of phase p that carries the applied "loads" and transfers the properties. The complementary fraction of finite (embedded) clusters or dead branches of phase p is $(1-\phi_p) f_p$. These two parts are related to the fraction of clustering and nonclustering (blocking) events, respectively [Torquato 2002]. We call ϕ_p and $1-\phi_p$ the *infinite* and *finite* cluster fractions of phase p, and likewise for phase q; the fractions ϕ_p and ϕ_q are independent and generally different.

[6]The isotropic analysis can be transposed to overall ellipsoidal symmetry for the material.

(i) When all fibers are infinite (total continuity of both phases), one has $\phi_p = \phi_q = 1$ and we denote $\boldsymbol{C}^{*\mathrm{IFS}}_{p|q}$ and $\boldsymbol{C}^{*\mathrm{IFS}}_{q|p}$ as the effective elastic moduli of these maximal IFSs, where the involved two homogeneous phases have moduli C_p and C_q. Taking these "IFS" effective moduli estimates as the effective moduli of the $p|q$ and $q|p$ planar sections of the two-phase material normally to any direction $\boldsymbol{\omega}$ will ensure the through-layers continuity of the p and q phases together with their ensured continuity normal to each $\boldsymbol{\omega}$ by the laminate structure. Any $\boldsymbol{\omega}$-oriented laminate system made of layers of these two phases, say $(a, b) = \begin{pmatrix} \mathrm{IFS} & \mathrm{IFS} \\ q|p & p|q \end{pmatrix}$, has effective moduli given by (2) or by (6) or (11a). The proportion of "phase a" (corresponding to matrix p having a continuous reinforcement of phase q) is $c_a = 1 - c_b$ (resp. b for matrix q continuously reinforced with p). An aggregate made of these two types of grains will also ensure the phase cocontinuity in the whole medium.

(ii) When one of the two phases, p or q, is in the totally embedded situation in the other phase, one has $\phi_p = 0$ or $\phi_q = 0$, respectively, since no infinite fibers exist. The effective properties of the corresponding layers (a) are the isotropic HS (IHS) bounds for the p matrix reinforced with the spherical inclusions taken to globally represent finite isotropic embedded clusters of phase q (resp. b for p in q). The calculation proceeds as in case (i), while taking $(a, b) = \begin{pmatrix} \mathrm{IHS} & \mathrm{IHS} \\ q|p & p|q \end{pmatrix}$ and the appropriate sphere GO_ϵ operator in (3). Effective moduli for laminates made of these two layer types are still given by (2), (6) or (11a). Note that piling sections which have isotropic effective moduli given by $\boldsymbol{C}^{*\mathrm{IHS}}_{p|q}$ and $\boldsymbol{C}^{*\mathrm{IHS}}_{q|p}$ is supposed to account for the limit of no through-section cocontinuity of the phases. However, it does not totally exclude this cocontinuity since in a layer of type (a) considered as embedding isotropic domains, connections with the matrix of phase q in adjacent layers of type (b) can be limit possible situations where single inclusions could link adjacent layers as shown with the small arrows in Figure 5, left. This makes a slight difference between the IPS and the ISC estimates, as defined, since assembling grains with these same $C^{*\mathrm{IHS}}_{p|q}$ and $C^{*\mathrm{IHS}}_{q|p}$ moduli more definitely excludes the cocontinuity of the phases p and q when one of the two phases is in dilute

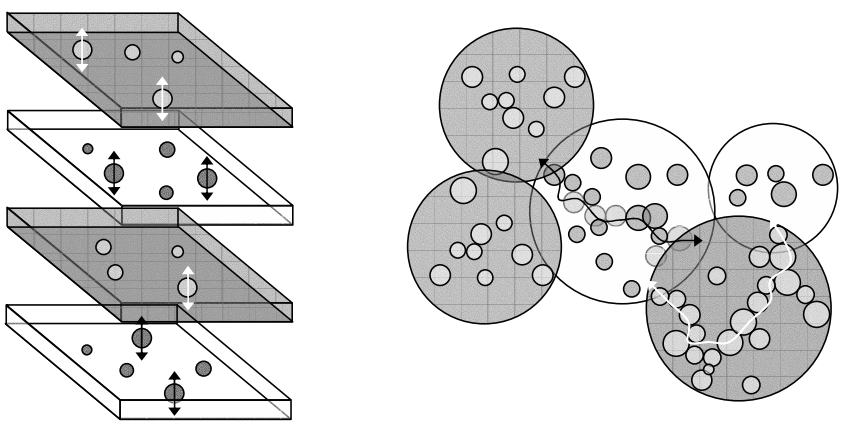

Figure 5. Situations of residual phase cocontinuity in the IPS layered construction (left) and the ISC aggregate construction (right).

concentration: when direct connections between grains of same phase are not enough, cocontinuity through grains of different types a and b would only happen if there exist, as in Figure 5, right, chains of domains q embedded in phase p which are at contact inside grains of type (a) such as to connect, along paths indicated by the arrows, with the matrix q of neighboring grains (b), which has a low probability of happening. This is a similar reasoning which yields to expect more reintroduction of dead branches in piling layers than in assembling grains at the opposite limit of total phase cocontinuity.

(iii) Partial phase cocontinuity possibilities correspond with $0 < \phi_p, \phi_q < 1$. We use a two-step homogenization procedure for successively "embedding" first the finite (spherical) domains that stand for all the finite clusters plus the dead branches and second the infinite fibers. For phase p in q the fraction $\kappa_p = (1-\phi_p) f_p \neq 1 - \kappa_q$ of spheres and the subsequent amount

$$\check{c}_p = \frac{f_p - \kappa_p}{1 - \kappa_p} \neq 1 - \check{c}_q$$

of infinite $\boldsymbol{\omega}$-fibers[7] in the modified matrix $\check{q}$ of moduli $\check{\boldsymbol{C}}_q$ (resp. for phase q in p), one has

$$\check{\boldsymbol{C}}^{*F(\omega)}_{p\subset q} = \check{\boldsymbol{C}}_q - \check{c}_p \big((\check{\boldsymbol{C}}_q - \boldsymbol{C}_p)^{-1} - (1-\check{c}_p) \boldsymbol{t}^{F(\omega)}_{\check{\boldsymbol{C}}_q} \big)^{-1}, \tag{18a}$$

$$\check{\boldsymbol{C}}_q = \boldsymbol{C}_q - \kappa_p \big((\boldsymbol{\Delta C}_{q|p})^{-1} - (1-\kappa_p) \boldsymbol{t}^{\mathrm{Sph}}_{\boldsymbol{C}_q} \big)^{-1}. \tag{18b}$$

The general IFS(ϕ) moduli estimate is then given by

$$\check{\boldsymbol{C}}^{\mathrm{IFS}(\phi p)}_{p\subset q} = \int_\Omega \frac{\check{\boldsymbol{C}}^{*F(\omega)}_{p\subset q}}{4\pi} \, \mathrm{d}\boldsymbol{\omega},$$

as in (17), which corresponds with $\kappa_p = \kappa_q = 0$, say $\check{c}_p = f_p = 1 - \check{c}_q = 1 - f_p$ in (18). The case of null cocontinuity corresponds with $\kappa_p = f_p = 1 - \kappa_q = 1 - f_q$, say $\check{c}_p = \check{c}_q = 0$. The infinite cluster fractions $\phi_i(f_i)$ of each phase (p, q) are similar to the continuous volume fractions of [Lee and Gurland 1978] (see [Ravichandran 1994; Fan 1995]) but are not the same: even when the continuous fractions reach unity, which corresponds with a single (necessarily sample spanning) cluster of each phase, the infinite cluster fraction $\phi_i(f_i)$ may remain smaller than unity because of the possibility of dead branches. But this is a detail.

The parameter $c_a = c^{0<\phi_q<1}_{a\equiv q\subset p}$ is the volume fraction of a phase cocontinuous material where the phase q is more alike a partially continuous reinforcement inside the matrix p than the opposite case (resp. for $c_b = c^{0<\phi_p<1}_{b\equiv p\subset q} = 1 - c_a$ when interchanging p and q). It clearly characterizes the cocontinuity asymmetry for the two phases (p, q) and we here call it the "clustering symmetry factor." In the limit case of no cocontinuity, $\phi_i(f_i) = 0$, it plays the same role of phase continuity inversion (or percolation transition) as the "matricity" parameter introduced by [Leßle et al. 1999], although not defined similarly. From now on, one will mainly examine the IPS-IFS and ISC-IFS estimates with

$$(a, b) = \begin{pmatrix} \mathrm{IFS}\,\phi_q & \mathrm{IFS}\,\phi_p \\ q|p & p|q \end{pmatrix},$$

[7] The second dilution of a volume fraction $\check{c}_p$ of phase p after a first dilution of volume fraction κ_p must match the total value f_p, accounting for the lost part $\check{c}_p \kappa_p$ due to overlapping inclusions (resp. q).

which read, from (15) and (16),

$$\boldsymbol{C}^{*\mathrm{IPSIFS}}_{(a,b,c_a)}(f_p) = \boldsymbol{C}^{\mathrm{IPSIFS}}_{a,b} = \langle \boldsymbol{C} \rangle + (\{\boldsymbol{C}\} - \boldsymbol{C}_a) : \boldsymbol{t}^{\mathrm{Sph}}_{\{\boldsymbol{C}\}} : (\{\boldsymbol{C}\} - \boldsymbol{C}_b), \tag{19a}$$

$$\boldsymbol{C}^{*\mathrm{ISCIFS}}_{(a,b,c_a)}(f_p) = \boldsymbol{C}^{\mathrm{ISCIFS}}_{a,b} = \langle \boldsymbol{C} \rangle + (\boldsymbol{C}^{\mathrm{ISCIFS}}_{a,b} - \boldsymbol{C}_a) : \boldsymbol{t}^{\mathrm{Sph}}_{\boldsymbol{C}^{\mathrm{ISCIFS}}_{a,b}} : (\boldsymbol{C}^{\mathrm{ISCIFS}}_{a,b} - \boldsymbol{C}_b). \tag{19b}$$

The infinite cluster fractions $0 \le \phi_p, \phi_q \le 1$ and the clustering symmetry factor $0 < c_a = 1 - c_b < 1$ may depend on the phase concentrations. The laws $c_a(f_p)$, $c_b(f_q)$ and $\phi_i(f_i)$, $i = p, q$ are expectedly monotonous increasing functions of the phase concentrations, but it is not impossible, as will be seen, to realize structures corresponding with decreasing evolution laws for $c_a(f_p)$, $c_b(f_q)$. The introduced phase continuity parameters are clearly related to phase clustering properties. Their definition is enough to allow measuring them, perhaps with the help of some tools from mathematical morphology and 3D image analysis. The precise relations of these parameters to the microstructural descriptors of systematic theory [Serra 1982; Torquato 2002] call for mathematical developments out of the present scope.

4.2. ***Phase concentration dependency assumptions for the phase continuity parameters.*** Considering phase concentration dependency makes sense in the cases when well-controlled structures can be realized at different phase concentrations without affecting any other property or characteristic. We use empirical forms to identify some general trends from comparisons with various data sets.

(i) For the independent infinite cluster fractions $\phi_p(f_p)$, $\phi_q(f_q)$, we have used

$$\phi_i(f_i) = \frac{\phi_{i0}(\phi_{i1}-\phi_{ik})\left(\dfrac{1-f_i}{1-f_{ik}}\right)^{P_i} + \phi_{i1}(\phi_{ik}-\phi_{i0})\left(\dfrac{f_i}{f_{ik}}\right)^{P_i}}{(\phi_{i1}-\phi_{ik})\left(\dfrac{1-f_i}{1-f_{ik}}\right)^{P_i} + (\phi_{ik}-\phi_{i0})\left(\dfrac{f_i}{f_{ik}}\right)^{P_i}} \quad i = p, q \tag{20a}$$

with, in general, $P_i > 0$ and $0 \le \phi_{i0} \le \phi_{ik} \le \phi_{i1} \le 1$. For all $P_i \ne 0$, the inflexion points have coordinates (f_{ik}, ϕ_{ik}) with $0 \le f_{pk}, f_{qk} \le 1$. When $P_i = 0$, the partial continuity of the phase is constant at ϕ_{ik}. The $\phi_i(f_i)$ functions are involved as a factor of (f_i). These two parameters should not be phase contrast dependent, which is a characteristic allowing to check the relevancy of their definition.

(ii) For the clustering symmetry factor $c_a(f_p) = 1 - c_b(f_q)$, we have used the similar form

$$c_a(f_p) = \frac{c_{ac}(f_p/f_{pc})^M}{c_{ac}(f_p/f_{pc})^M + c_{bc}(f_q/f_{qc})^M} = 1 - c_b(f_q), \quad f_{pc} + f_{qc} = 1, \quad c_{ac} + c_{bc} = 1 \tag{20b}$$

For all $M \ne 0$, the inflexion point has coordinates $f_{pc} = 1 - f_{qc}$, $c_{ac} = 1 - c_{bc}$. When $M = 0$, the value of c_{ac} fixes the estimate position between the limits IFS(ϕ), for all f_{pc}. When $M > 0$, the transition is from the lower limit to the upper one, and the opposite occurs for $M < 0$. The larger is the value of $|M|$, the sharper the inversion of the cocontinuity symmetry at that point. The variation of this clustering symmetry factor form can be expected to be dependent of the phase contrast because in our two-scale homogenization scheme, it interconnects intermediate IFS(ϕ) phases $(\boldsymbol{C}_a, \boldsymbol{C}_b)$ which are not of constant microstructures (as they are made from mixing the constitutive ones (p, q) with concentration-dependent $\phi_p(f_p)$ and $\phi_q(f_q)$ continuity characteristics).

5. Result comparisons with numerical and experimental data

The so-defined generalized IFS(ϕ) estimates are taken for the effective properties of the two representative layers in IPS descriptions for two-phase materials from (19a). They are taken as well for the effective properties of the two representative spherical domains in isotropic self-consistent (ISC) descriptions of the same materials from (19b). Note that planar sections of such two-phase aggregates are 2D patchworks of the same two types of domains as those directly introduced in the layer-based approach. The IFS aggregate is expected to be phase cocontinuous at all concentrations provided $\phi_p, \phi_q \neq 0$, as both grain types are phase cocontinuous in that case. The IPS that reassembles sections of IFS aggregates is also expected to be phase cocontinuous at all concentrations when $\phi_p, \phi_q \neq 0$ but possibly with some residual bicontinuity when $\phi_p = \phi_q = 0$ in the layers, as described in Figure 5, and similarly some dead branches are reintroduced when $\phi_p = \phi_q \to 1$. It will be shown, indeed, that the two obtained IPS-IFS and ISC-IFS estimates are identical for the various examined structures when phase bicontinuity in the IFSs is significant and high (no apparent difference towards total bicontinuity), while in situations of vanishing bicontinuity in the IFSs, the ISC estimate involving IHS grains is slightly sharper than the IPS estimate using IHS layers.

Table 3 presents the genealogy of the calculated and compared estimates that are linked in columns from the phase pairs (a, b), the pair Voigt–Reuss(a, b), the pair IHS(+/-)(a, b) and the pair IFS(+/-)(a, b). The estimate from (13) for the aggregate of laminates denoted "ISCP" has been placed in a remaining free cell of the table. The total number of examined estimates is 15, including some cases that have been pointed out as inconsistent with the possible cocontinuity of the phases (namely, the IPS estimates combining either V and R layers or IHS$(+/-)$ layers, and the ISC estimates combining either V and R grains or IHS$(+/-)$ grains). The analytic expressions for the effective shear modulus in the incompressible case (for the two phases a, b) are summarized in Appendix C for the IFS, IPS, IHS and ISC estimates, plus, as a sixteenth estimate, the dual IPS one from the compliance approach of (11b). Typical curves for all of the IPS and ISC estimate types that have been considered are plotted in the left and middle

a/b	VR(a, b)	isotropic HS(a, b)	fiber HS(a, b)
ISC[P$\omega(a, b)$]			isotropic FS[FHS(a, b)]
laminate $[a/b]$	laminate [VR(a, b)]	laminate [IHS(a, b)]	laminate [IFS(FHS(a, b))]
isotropic PS[L(a, b)]	isotropic PS[L(VR(a, b))]	isotropic PS[L(IHS(a, b))]	isotropic PS[L(IFS(FHS(a, b)))]
isotropic SC$[a, b]$	isotropic SC[VR(a, b)]	isotropic SC[IHS(a, b)]	isotropic SC[IFS(FHS(a, b))]

Table 3. Genealogy of the 15 estimates performed. and notations. VR = Voigt–Reuss; HS = Hashin–Shtrikman; FHS = fiber HS = HS bounds for (a,b) 1D-fiber structures; FS = fiber systems; L = laminate structure; PS = platelet Systems; SC = self-consistent estimate; IHS, IFS, IPS, ISC = isotropic HS, FS, PS, SC.

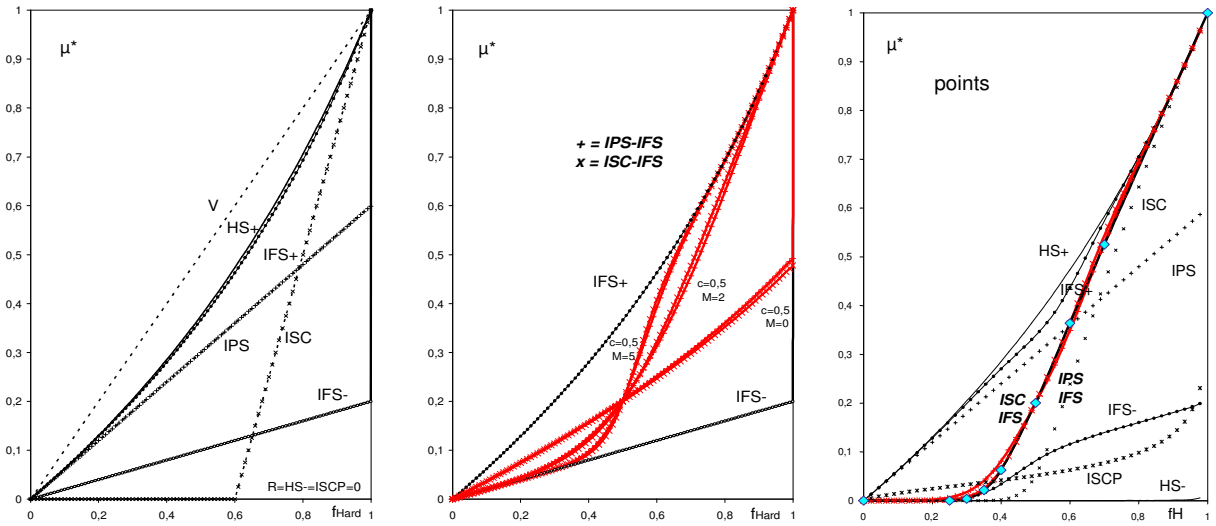

Figure 6. Comparison of moduli estimates for porous materials. Left: estimates not involving (20). Middle: IFS limits and related IPS-IFS and ISC-IFS estimates for $M = 0$, $M = 2$, and $M = 5$. Right: Matching the FFT estimate for a point structure with the IPS-IFS and ISC-IFS estimates.

portions of Figure 6 for an incompressible two-phase material with a void phase, say ($\nu_p = \nu_q = 0.5$), ($\mu_q/\mu_p = 0$). To save space, the rightmost part of Figure 6 reports with some anticipation the match of the IPS-IFS and ISC-IFS estimates with an FFT calculation on a simple point structure in the case of nearly zero contrast: $\mu_q/\mu_p = 5 \times 10^{-5}$ (see Figure 7, left, on page 749, for an illustration).

Figure 6, left, shows plots of the 9 estimates obtained from the pure phases (p, q), namely, the V/R bounds and the two IHS bounds, the IPS, the ISC and the ISCP estimates and the two IFS limits at $\phi_p = \phi_q = 1$. The upper IFS estimate, $\mu_{\mathrm{IFS}(+)} = (1 + \frac{1}{5} f_q) f_p \mu_p/(1 + f_q)$, is closely below the upper IHS bound $\mu_{\mathrm{IHS}(+)} = 3 f_p \mu_p/(3 + 2 f_q)$. The nonzero lower IFS estimate, $\mu_{\mathrm{IFS}(-)} = \frac{1}{5} f_p \mu_p$, is far above the IHS lower bound that is zero when $f_p \neq 1$. The IPS estimate, $\mu_{\mathrm{IPS}} = \frac{3}{5} f_p \mu_p$, is between the two IFS limits in all of the phase concentration range, going from the upper IFS limit to the lower one. From Appendix C, μ_{IPS} and $\mu_{\mathrm{IFS}(-)}$ make a singular jump from respectively $\frac{3}{5}$ and $\frac{1}{5}$ to 1 at $f_p = 1$. When the phase q is a void phase, neither the ISC estimate (which is linear from 0 to μ_p between $f_p = \frac{2}{5}$ and 1) nor the ISCP estimate (which goes to zero at all concentrations $f_p \neq 1$) remain between the IFS limits for all concentrations or for all contrasts.

The dual IPS estimate from the arithmetic mean over compliances, not plotted but given in Appendix C, also remains close to the IHS lower bound and goes to zero in the void phase case. Figure 6, middle, illustrates the flexibility of the two IPS-IFS and ISC-IFS estimates by reporting a typical case of no phase concentration dependency ($M = P_1 = P_2 = 0$, $c_{ac} = c_{bc} = 0.5$, $\phi_{pk} = \phi_{qk} = 1$) and examples of phase concentration dependency for $M = 2$ and $M = 5$. They correspond to the cases denoted by 000 and MPP in Table 4 (page 751), which summarizes all of the parameter values for the performed calculations presented next. The same graph also shows the close proximity of these two estimates arising from two different routes in a few representative cases. The simultaneous match, in Figure 6, right, of the

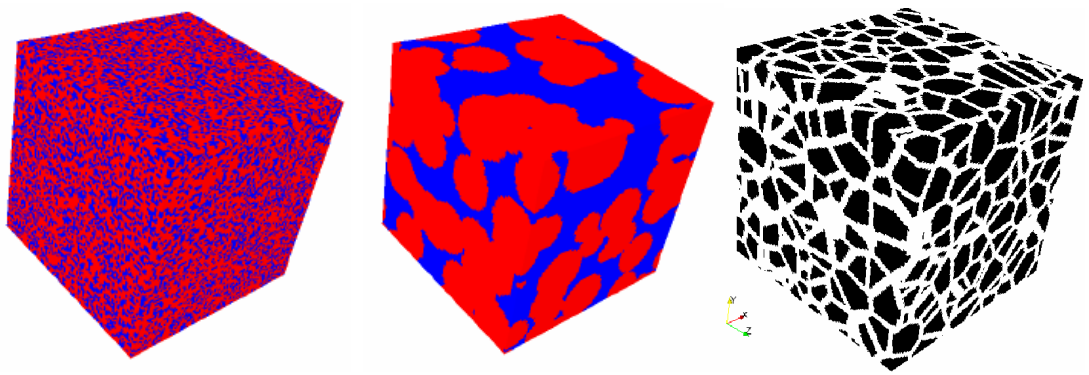

Figure 7. Numerical structures of random points (left), overlapping spheres (middle), and Voronoi cells (right).

IPS-IFS and ISC-IFS estimates with the FFT calculation for the point structure, has needed the use of nonconstant ϕ functions ($P_i = 4$); this is because, as expected, point structures are only bicontinuous in the range of comparable concentrations of the two phases, with the continuity of each phase increasing with its concentration. The already-marked stiffness of the ISCP estimate at this still high contrast, compared to the still nearly zero IHS lower bound, is noteworthy. Figures 7, 8 and 9 illustrate the various numerical or real structures for which available moduli calculations or measurements have been compared to the proposed IPS-IFS and ISC-IFS estimates and to some of the other ones. Figures 10–13 report the performed estimate comparisons of the (shear or Young) effective moduli.

5.1. ***Structure types investigated.*** The three parts of Figure 7 show numerical structures obtained by random point processes. The elementary cube has 128^3 voxels. In the point structure of Figure 7, left, the point number is directly the second phase volume part. In the middle figure, they are the centers of overlapping spheres having all the same radius. In the rightmost figure they are cell centers from which Voronoi structures with different wall thicknesses are built. The overlapping sphere arrangement is known to have a quite large and asymmetric domain of cocontinuity (from 0.30 to 0.95, approximately). The phase contrast inversion matters in this case. This sphere structure is varied in concentration by modifying the sphere radius. The Voronoi cell structure is expected to have, at all phase concentrations, a continuous wall phase separating polyhedral inclusions, without any bicontinuity. The phase concentration is varied by changing the wall thickness and the grain number. If holes happen in walls that are too thin, such Voronoi structures can turn into bicontinuous ones. Piercing or removing walls is a way to create bicontinuous structures.

The parts of Figure 8 present the different phase arrangements obtained from a Poisson–Voronoi tessellation process. Figure 8, left, is obtained by removing the cell faces in a Voronoi structure, just keeping the edges and vertices that remain connected into a continuous second phase reinforcement. This is typically a bicontinuous structure that is expected to be totally bicontinuous (TBi). When the walls are too thin (middle figure), edges can be broken when removing the faces, which yields partial bicontinuity (dead branches in the continuous reinforcement) and possibly a phase continuity inversion with a connected matrix including discontinuous reinforcements (PBi/I). When conversely the walls are too thick (right figure), edges and vertices dominate and there are not enough face points left to connect

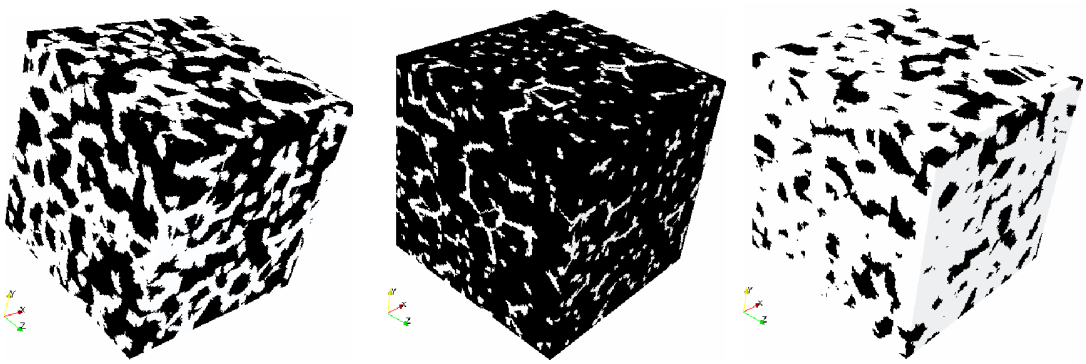

Figure 8. Bicontinuous structures. Left: removing wall faces of Voronoi cells. Middle: partial or inverted phase continuity if thin wall edges have been broken. Right: Voronoi type if walls are too thick.

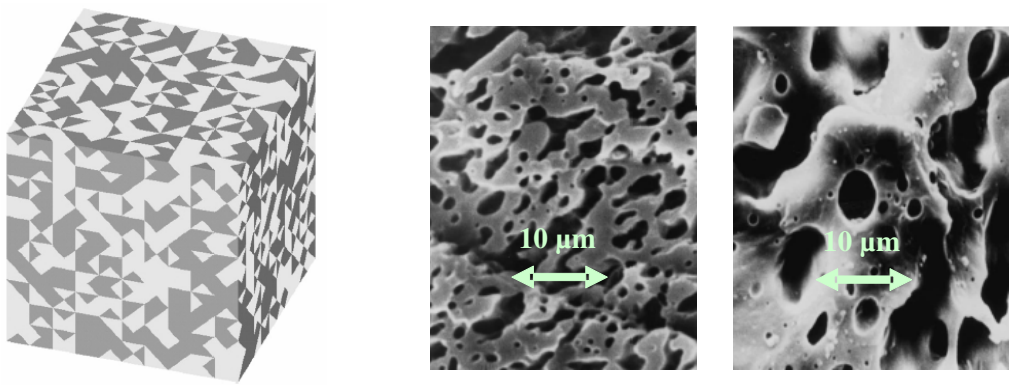

Figure 9. Left: numerical bicontinuous structure of [Chen et al. 2008]. Middle, right: PS and PP bicontinuous polymer blends prepared and examined by Veenstra et al. [2000].

the cell phase by piercing the walls. The structure remains of the Voronoi cell structure type, with only some finite clusters of connected cells and no bicontinuity. Estimates for Voronoi cell structures are not reported.

Figure 9 illustrates some examined structures taken from the literature. The diagram on the left, from [Chen et al. 2008], is a numerical structure of the nonparticulate type created from a random point process that results in an intermediate range of phase bicontinuity. FEM calculations of the effective Young modulus have been reported for moduli values given to the phases that are typically those of an epoxy-glass mixture ($\mu_p = 1,26\,\text{GPa}$, $\nu_p = 0.35$), ($\mu_q = 30\,\text{GPa}$, $\nu_q = 0.22$). The other two parts of Figure 9 are views of two types of polymer blends prepared and investigated by Veenstra et al. [2000]. The two materials (PS and PP for, respectively, blends of polyethylene with poly(ether-ester) and blends of polypropylene with styrene (ethylene-butylene)) exhibit a phase cocontinuity domain of variable extent where their structures are typically sponge-like, as exemplified in the figure. For comparisons with the two PS blends (denoted PSi and PSs), we used $E_p^{\text{PS}} = 2800\,\text{MPa}$, $E_q^{\text{PS}} = 48\,\text{MPa}$, and for the two PP

blends (PPi and PPs), we used $E_p^{\mathrm{PP}} = 1000\,\mathrm{MPa}$, $E_q^{\mathrm{PP}} = 3\,\mathrm{MPa}$. Since the phase Poisson ratios were not given, we used an arbitrary homogeneous value, which does not matter because the Young's and shear moduli are proportional then. However, the assumption of the same Poisson ratio for both phases makes these comparisons more uncertain. The estimates for these structures are reported versus the hard (PS or PP) phase concentration.

5.2. *Main results and discussion.*

Estimated effective moduli and comparisons. According to the case, either the estimated effective shear modulus or the effective Young's modulus (normalized in the case of Chen data) has been reported for the various mentioned models. Most of the calculated moduli estimates for the structures of Figure 7 and 8 assume the same incompressible phases $\nu_p = \nu_q = 0.5$ with a contrast ($\mu_q/\mu_p = 4 \times 10^{-3}$) for the shear moduli. Some calculations with a weaker or a higher contrast for the phase shear moduli (between 0.1 and 0) were also performed for further discussion. For comparisons, the shear effective modulus was calculated by using the FFT method as detailed in [Brenner et al. 2009] for its implementation. For the IPS-IFS and ISC-IFS estimates, we collect in Table 4 the phase continuity parameters involved in (20) that have provided a good match with the compared data sets. No numerical algorithm of fitting parameter identification has been called for because our discussion purpose does not need a perfect matching.

Figures			M	f_{ac}	c_{ac}	P	$\phi_{\min}$	$\phi_{\max}$	ϕ_k	f_{pk}	f_{qk}
REF 000		6 middle	0		0.5	0	0	1	0.5		
REF MPP		6 middle	2 and 5	0.5	0.5	4	0	1	0.5	0.5	0.5
FFT PTS	7 left	6 right	3	0.45	0.5	4	0	1	0.5	0.45	0.45
Match ISC		10 left	2	0.5	0.5	9	0	1	0.5	0.5	0.5
Match IPS		10 middle	−0.33	0.5	0.8	0	1	1	1	0.5	0.5
Match ISCP		10 right	−0.25	0.5	0.5	1	1	0	0.5	0.5	0.5
FFT h SPH	7 middle	11 right	1.5	0.65	0.5	1.5	0	1	0.5	0.65	0.65
FFT s SPH	7 middle	11 middle	1.5	0.35	0.5	1.5	0	1	0.5	0.35	0.35
FFT vo SPH	7 middle	11 left	2.1	0.35	0.5	1.5	0	1	0.5	0.35	0.35
FEM CHen	9 left	12 left	1.5	0.6	0.7	5	0	1	0.5	0	0
FFT TBi	8 middle	12 middle	0.5	0.7	0.7	1.5	0.25	0.75	0.5	0.5	0.5
FFT PBi/I	8 right	12 right	2	0.5	0.5	3	0.25	0.75	0.5	0.5	0.5
Exp VE PSi	9 middle	13 top left	5	0.45	0.5	3	0	1	0.5	1	1
Exp VE PSs	9 middle	13 top right	4	0.3	0.5	3	0	1	0.5	0.7	0.9
Exp VE PPi	9 right	13 bottom left	0.4	0.97	0.7	10	0	1	0.5	0.5	0.6
Exp VE PPs	9 right	13 bottom right	0.3	0.97	0.7	15	0	1	0.5	0.45	0.55

Table 4. Coefficients for the IPS-IFS and ISC-IFS moduli estimates to match with compared data and notation (the columns P, $\phi_{\min}$, $\phi_{\max}$, ϕ_k refer to both phases). For REF 000 and REF MPP, see page 748. ISCP = ISC estimate on PS systems from (13). TBi/PBi = totally/partially bicontinuous (see page 749). PTS = point structure. EXP VE PS(i/s)/PP(i/s) = experimental data on polymer blends from [Veenstra et al. 2000]. FEM CHen = numerical data from [Chen et al. 2008]. (h/s/vo) SPH = hard/soft/void-like spherical inclusions.

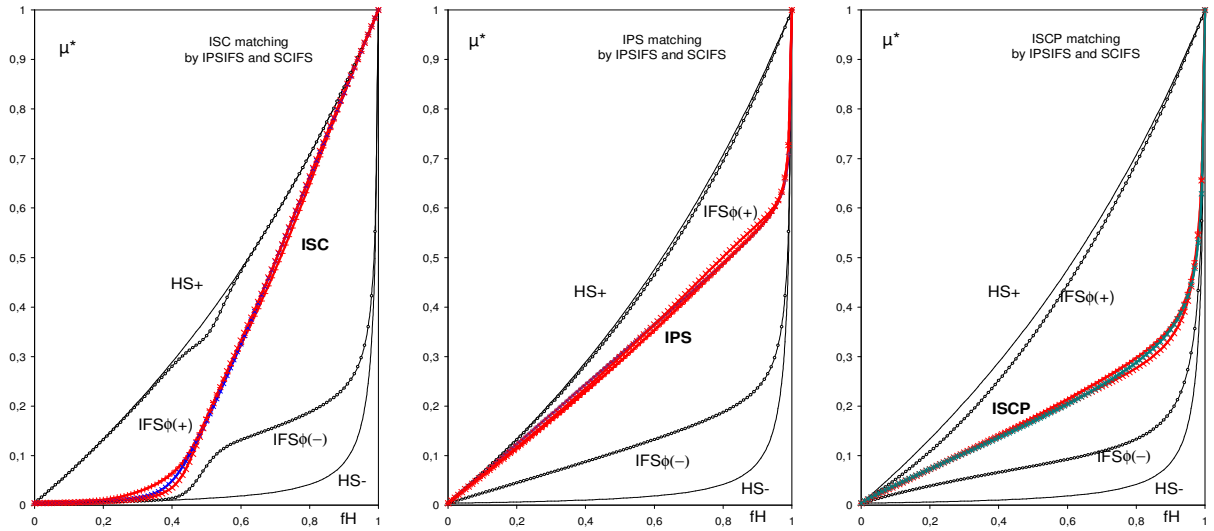

Figure 10. Matching the ISC, ISCP and IPS estimates with the IPS-IFS and ISC-IFS ones.

Figure 10 compares the ISC, IPS and ISCP analytical estimates with the IPS-IFS and ISC-IFS ones adjusted with an appropriate set of parameters. These comparisons provide preliminary information about the ranges of parameter values to be explored according to the case. In particular: the ISC estimate is of the types of reference MPP reported in Figure 6, middle, and it is not much different from the point structure (Figure 6, right) considering statistical fluctuations; the IPS estimate that goes from the upper IFS limit to the lower one is matched by using a negative value for the power M and by keeping the ϕ_i functions constant and equal to unity (total constant cocontinuity); the ISCP estimate is also matched with using a negative M value while furthermore making the ϕ_i functions to decrease from unity to zero, as if corresponding to the dilute phase gaining total continuity when vanishing while the dense one has vanishing continuity when approaching unity. This can be understood as going towards a zero phase concentration under the form of a vanishing but still sample spanning and total cluster.

Figure 11 shows a comparison with the FFT computations on the sphere structures of Figure 7, middle, considering two different phase contrasts for the soft sphere case in a hard matrix (left and middle) and the dual structures with soft and hard spheres (middle and right). Figure 12, left, reports the estimates that match the FEM calculations of [Chen et al. 2008] for the numerical (point-like) structure of Figure 9, left, (normalized Young's moduli), a case of moderate phase contrast ($E_q/E_p \approx 0.045$). The remaining two parts of Figure 12 report the estimate for the structures of the corresponding parts of Figure 8, compared with the FFT calculations. The four parts of Figure 13 match the estimates with the measured values for the PSi, PSs, PPi, and PPs blends from [Veenstra et al. 2000], corresponding to the last two parts of Figure 9. The contrasts, respectively, are $E_q/E_p \approx 0.015$ and $E_q/E_p \approx 0.003$. The concentration ranges of cocontinuity experimentally estimated are respectively 0.5–0.6, 0.3–0.6, 0.5–0.6 and 0.4–0.8, say: larger for the (s) samples than for the (i) ones.

Figure 11 and 12 (parts a and c) show estimates of the reference MPP type, corresponding to a bicontinuity domain between two domains where the dilute phase is expected to be embedded in the concentrate one. Note that the two dual sphere structures (last two parts of Figure 11) are nicely fitted

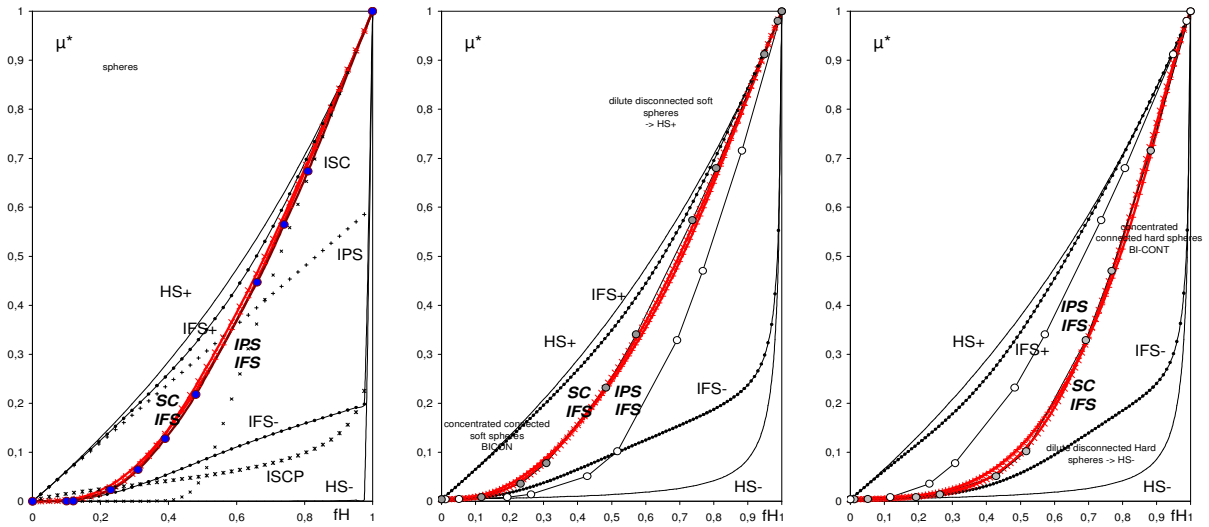

Figure 11. Matching FFT calculations with the IPS-IFS and ISC-IFS estimates for the sphere structure. From left to right: void-like, soft, and hard spheres.

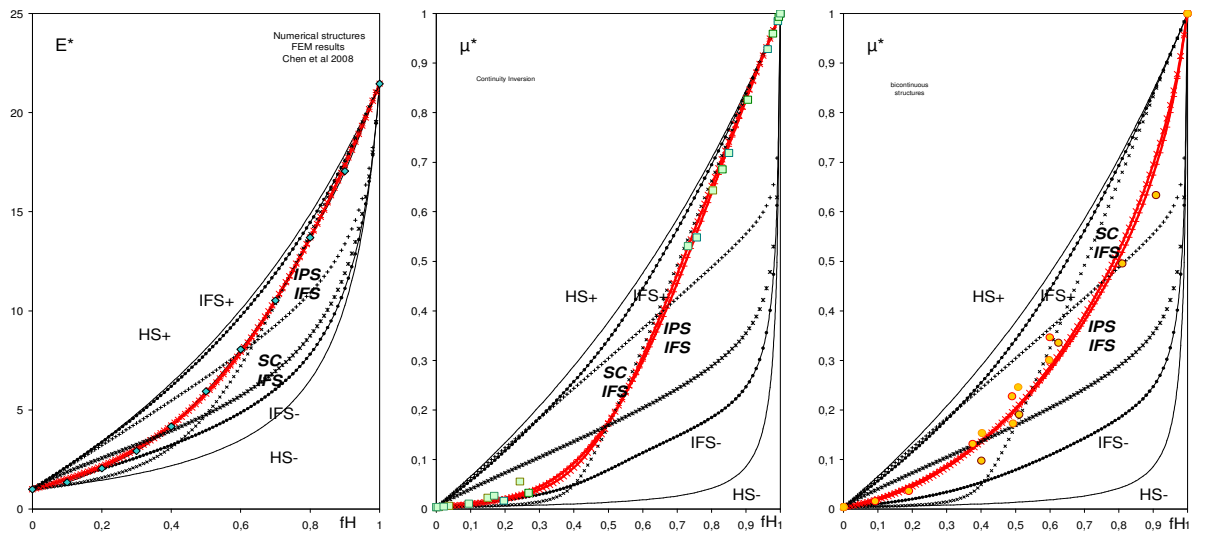

Figure 12. Left: matching the numerical FEM calculations of [Chen et al. 2008, Figure 3] with the IPS-IFS and ISC-IFS estimates. Middle and right: matching the FFT calculations for totally and partially bicontinuous Voronoi-based structures with the IPS-IFS and ISC-IFS estimates.

by the same parameter set, only inverting the value of the critical concentrations (0.35 / 0.65) in (20a) and (20b). The case of Figure 12, middle, although of the same structure type, corresponds to a smaller M value and some other distinct parameter values. In all of these cases, the IFS(ϕ) domain that limits the data set is regular thanks to a low value of P in (20b), as collected in Table 4.

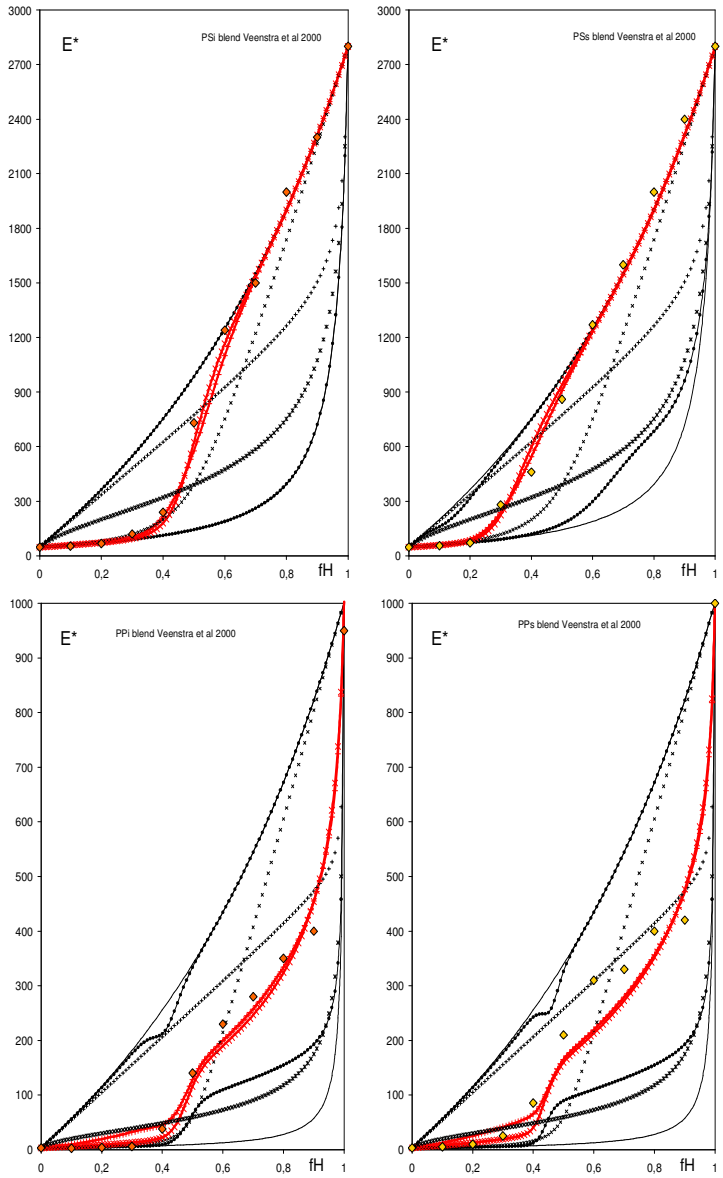

Figure 13. Matching the blend data of [Veenstra et al. 2000, Figure 3] with the IPS-IFS and ISC-IFS estimates. Top row: lower and upper data of Figure 3, left. Bottom row: lower and upper data of Figure 3, right.

The PS and PP polymer blends exhibit two radically different situations compared to the previous ones. For the PS case, the match of the data again corresponds to a typical MPP curve, although with a higher M value (of 5 and 4, respectively, for cases PSi and PSs), in order to give an S shape to the curve corresponding to $M = 5$, as in Figure 6, middle. The PP blends show the particularity of a modulus "jump" when approaching a zero weak-phase concentration, while the PS blends do not. For this PP

case, the "best match" of the data we have obtained with (20), which is not as good as in the other cases, corresponds with a very different set of parameters. In particular, the S shape that has been given to the ϕ curves of (20b) has used high P values and low M values, with inflexion points very far from symmetrical. Although the compared experimental data for PP blends are more uncertain than the other data (at dilute concentrations of the hard phase, some points are not even between the V/R bounds), such a jump to 1 of $\phi_p(f_p)$ when f_p approaches 100% is in agreement with still partial continuity (dead branches) of the hard phase when dense and persisting up to the total vanishing of the soft phase. It is interestingly a case for which the Christensen's IPS estimate appears quite convenient for a dominant volume fraction of the hard phase what means a still significantly continuous soft phase when dilute, especially for the PPs case that exhibits the largest concentration range of phase of bicontinuity. This IPS estimate is thus proved possibly relevant for this type of materials with cocontinuous phases. It is also noteworthy that for these parameter sets in the PP cases, a quite marked difference appears between the IPS-IFS and ISC-IFS estimates in the domain of dilute hard phase, where the estimates remain more of the IPS-IHS and ISC-IHS type ($\phi_p, \phi_q \approx 0$), with nearly no cocontinuity in the representative layers or grains (as described by the high values given to P and to f_{pc}). Accordingly with the difference in their definitions, the IPS-IFS estimate appears smoother than the ISC-IFS, likely in relation to some maintained phase bicontinuity. At the other end, when assuming total continuity by $\phi_p = \phi_q = 1$, one could expect for the same reason of construction difference some more dead branches being reintroduced in piling layers than in assembling grains, but one does not observe a significant difference between the IPS-IFS and the ISC-IFS estimates then. This yields to considering the IPS-IFS estimate as a smoothed version of the ISC-IFS one, especially when the infinite cluster fractions ϕ_p, ϕ_q approach either 0 or 1.

Phase contrast dependency. We end with these comparisons by checking whether the parameters in (20) depend on the phase contrast or not. As far as they represent morphological characteristics, they should be insensitive to the phase contrast in all the cases where the phase composition do not change with the phase concentration and arrangement. In that respect, the phase concentration dependency of the infinite cluster fractions $\phi_p(f_p)$ and $\phi_q(f_q)$ from (20a) that characterizes the morphology of the individual phases is not expected sensitive to phase contrast, oppositely with the variation of the clustering symmetry factor from (20b).

Using the set of parameters given in Table 4, the ISC, IPS and ISCP analytical curves and the FFT results for the soft sphere structure have been matched with the IPS-IFS and the ISC-IFS estimates for different phase contrasts ranging between 0.1 and 0.00005. The net result is that the match remained of similar accuracy, by only modifying the M exponent in (20b) as shown in Figure 14, where the logarithmic plot looks linear, and all other parameters that concern (20a) remaining unchanged[8]. Reporting the miscellaneous data for M corresponding to other calculations with a single available contrast case confirms that the Chen et al. data, the PBi/I data and the ISC plot are similar to the point-structure data type. Going towards an increase of bicontinuity, as the sphere structures and the totally bicontinuous (TBi) structures, seems to correspond with a lower but still positive M value. Negative M values for the IPS and ISCP estimates may also correspond to realizable bicontinuous structures, as with aggregates of laminate domains. In terms of M value, the PP blends are on the side of the bicontinuous structures, while the PS ones are quite far above all estimates.

[8]Also the inflexion point (f_{pc}, c_{ac}) can need a slight adjustment when the phase contrast becomes weak.

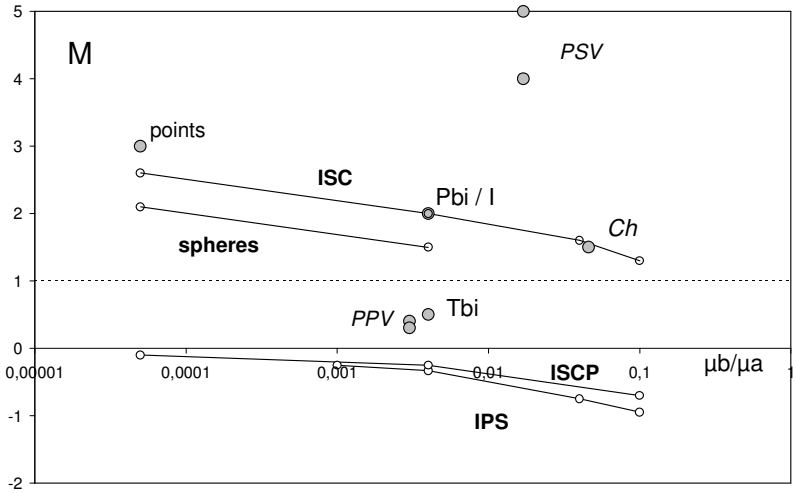

Figure 14. The variation of the M parameter with phase contrast for the different estimates.

The PP and PS blend cases warn that one cannot only compare the M parameter in order to classifying the structure types but this comparison nevertheless provides interesting information on the different possible types of phase cocontinuous structures.

Without going more deeply into the details here, it appears from these elements that some typical trends of phase cocontinuity show up for the different microstructures that have been examined through the presented two not much different modeling schemes. The parameter sets that provide a good match with the available data are related to cluster characteristics and percolation features of the phases, here called the infinite cluster fractions and the clustering symmetry factor. They are measurable quantities but remain to be connected appropriately to the microstructural descriptors. The fact that one nearly obtains by two routes using the same representative domains of IFS estimates, the same estimate for the considered bicontinuous structures can be taken in favor of the relevancy of the given description to the representative, layers or grains, domains. While the ISC-IFS estimate is implicit owing to the SC approximation level in it, the layer-based IPS-IFS estimate remains explicit. Towards null phase bicontinuity, the layer-based approach yields a slightly smoother estimate than the aggregate one, likely related to a residual phase cocontinuity not totally excluded in the layer approach. Conversely, total phase cocontinuity in layers does not either totally exclude the reintroduction of dead branches when assembling the layers, but there is no noticeable difference between the two estimates in that case. These modeling schemes, which have been presented in details in the elasticity formalism in specifying which application restrictions should be kept in mind in the mechanical field, also hold to estimating physical effective properties in all situations for which the homogenization framework holds. The calculation of the IFS estimates is possible for any phase number, and so are the IPS-IFS and ISC-IFS estimates when following the same procedure as for two phases. As will be soon presented elsewhere, (19) can be directly applied to arrangements of isotropic phases in ellipsoidal overall symmetry while using the appropriate operator for the characteristic ellipsoidal shape. They also likely apply as written in the cases of anisotropic structures involving anisotropic phases, as the morphological background to account for phase continuity features remains unchanged.

6. Conclusion

We have proposed, within the homogenization framework, a modeling scheme which aims at estimating the effective properties of heterogeneous materials which exhibit a diversity of phase cocontinuity features for several of their constitutive phases. For mechanical properties, our approach is restricted to the study of elasticity properties in the unloaded limit and to materials whose structural behavior under load is not essentially governed by bending or torsion features. The modeling results from the use of a generalization of the so-called fiber systems combined within either a layer-based or an aggregate-like approach to describe the material structure and on the introduction of phase clustering characteristics as phase continuity and cocontinuity parameters. As shown for two-phase materials in the isotropic elastic formalism, the two obtained estimates are very close to each other for all examined microstructures over the whole phase concentration range where they present significant phase bicontinuity and regardless of the phase contrast. In situations when the phase cocontinuity is weak or null, the layer-based estimate appears to be slightly smoother than the aggregate-based one because of some residual phase cocontinuity not totally excluded by the estimate construction. The various performed comparisons with the experimental and numerical data from the literature and with the FFT calculations performed on different numerical microstructures have shown the high flexibility of the modeling and its ability to consider phase cocontinuity characteristics of a large variety of situations. Since, as stressed from the introduction, platelet (or laminate), aggregate and fiber systems can be defined for multiphase materials whose phases are of general property anisotropy and are assembled according to an ellipsoidal overall symmetry, as being presented in a separate work, the application domain of the two proposed estimate types can be extended accordingly.

Appendix A. Platelet Green operators and moduli and compliance tensors for laminates

The fundamental property of the platelet strain Green operator. From [Walpole 1981], one has

$$\big(\boldsymbol{I} - t^P_{(p)}(\omega) : (\boldsymbol{C}^p - \boldsymbol{C}^q)\big) : \big(\boldsymbol{I} - t^P_{(q)}(\omega) : (\boldsymbol{C}^q - \boldsymbol{C}^p)\big) = \boldsymbol{I} \tag{A.1}$$

for any two phases p, q and any direction $\boldsymbol{\omega}$ in space. This property also corresponds to

$$\boldsymbol{I} = \big(t^P_{(p)}(\omega) : (\boldsymbol{C}^p - \boldsymbol{C}^q)\big)^{-1} + \big(t^P_{(q)}(\omega) : (\boldsymbol{C}^q - \boldsymbol{C}^p)\big)^{-1} \tag{A.2}$$

Thus allows one to write, for all $f_q = 1 - f_p$, the equality $\boldsymbol{C}^{*P\omega}_{q\subset p} = \boldsymbol{C}^{*P\omega}_{p\subset q}$ for a two-phase laminate as

$$\boldsymbol{C}^p - f_q\big((\boldsymbol{C}^p - \boldsymbol{C}^q)^{-1} - f_p t^P_{(p)}(\omega)\big)^{-1} = \boldsymbol{C}^q - f_p\big((\boldsymbol{C}^q - \boldsymbol{C}^p)^{-1} - f_q t^P_{(q)}(\omega)\big)^{-1} \tag{A.3}$$

One backward demonstration results from multiplying (A.3) by $(\boldsymbol{C}^p - \boldsymbol{C}^q)^{-1}$ to obtain

$$\begin{aligned}\boldsymbol{I} &= f_q\big(\boldsymbol{I} - f_p t^P_{(p)}(\omega) : (\boldsymbol{C}^p - \boldsymbol{C}^q)\big)^{-1} + f_p\big(\boldsymbol{I} - f_q t^P_{(q)}(\omega) : (\boldsymbol{C}^q - \boldsymbol{C}^p)\big)^{-1}\\ &= f_q(\boldsymbol{I} - \boldsymbol{X}_p)^{-1} + f_p(\boldsymbol{I} - \boldsymbol{X}_q)^{-1},\end{aligned}$$

which yields $f_q\big(\boldsymbol{I} - (\boldsymbol{X}_q)^{-1}\big) + f_p\big(\boldsymbol{I} - (\boldsymbol{X}_p)^{-1}\big) = 0$ and (A.2).

The symmetric form of the effective properties of two-phase laminates. The tensor $\boldsymbol{C}^{*P\omega}_{q\subset p}$ reads

$$\boldsymbol{C}^p - f_q\big((\boldsymbol{C}^p-\boldsymbol{C}^q)^{-1} - f_p\boldsymbol{t}^P_{(C^p)}(\omega)\big)^{-1} = \boldsymbol{C}^p - f_q(\boldsymbol{C}^p-\boldsymbol{C}^q):\big(\boldsymbol{I}-f_p\boldsymbol{t}^P_{(C^p)}(\omega):(\boldsymbol{C}^p-\boldsymbol{C}^q)\big)^{-1}.$$

Using the homogeneity of rank -1 of $\boldsymbol{t}^V_{(\boldsymbol{C}^p)}$ with respect to the moduli $f_p\boldsymbol{t}^P_{(\boldsymbol{C}^p)}(\omega) = \boldsymbol{t}^P_{(\boldsymbol{C}^p/f_p)}(\omega)$ and setting $\boldsymbol{C}^p-\boldsymbol{C}^q = \boldsymbol{C}'^p - \boldsymbol{C}^{*q}$ with $\boldsymbol{C}'^p = \boldsymbol{C}^p/f_p$, $\boldsymbol{C}^{*q} = \{\boldsymbol{C}\}/f_p$, yields

$$\big(\boldsymbol{I}-f_p\boldsymbol{t}^P_{(\boldsymbol{C}^p)}(\omega):(\boldsymbol{C}^p-\boldsymbol{C}^q)\big)^{-1} = \big(\boldsymbol{I}-\boldsymbol{t}^P_{(\boldsymbol{C}'^p)}(\omega):(\boldsymbol{C}'^p-\boldsymbol{C}^{*q})\big)^{-1} = \boldsymbol{I}-\boldsymbol{t}^P_{(\boldsymbol{C}^{*q})}(\omega):(\boldsymbol{C}^{*q}-\boldsymbol{C}'^p).$$

The last form results from the platelet property. Using $\boldsymbol{t}^P_{(\boldsymbol{C}^{*q})}(\omega) = f_p\boldsymbol{t}^P_{\{\boldsymbol{C}\}}(\omega)$, we arrive at

$$\boldsymbol{C}^p - f_q(\boldsymbol{C}^p-\boldsymbol{C}^q):\big(\boldsymbol{I}-f_p\boldsymbol{t}^P_{(\boldsymbol{C}^p)}(\omega):(\boldsymbol{C}^p-\boldsymbol{C}^q)\big)^{-1} = \boldsymbol{C}^p - f_q(\boldsymbol{C}^p-\boldsymbol{C}^q):\big(\boldsymbol{I}-f_p\boldsymbol{t}^P_{\{\boldsymbol{C}\}}(\omega):(\boldsymbol{C}^q-\boldsymbol{C}^p)\big)$$

and to (6), (11a) as well as to (9), (11b) for $S^{*P}(\omega) = (C^{*P}(\omega))^{-1}$. Note that $\{\boldsymbol{S}\}\neq\{\boldsymbol{C}\}^{-1}$.

Appendix B. Properties of the Hashin–Shtrikman (HS) and self-consistent (SC) estimates

The HS estimates. The general form is given in (2) and (3). In the two-phase case, the proof that $\boldsymbol{C}^{\text{eff HS}}_{p\subset q} = \boldsymbol{C}^q - f_p\big((\boldsymbol{\Delta C}^{q|p})^{-1} - f_q\overline{\boldsymbol{t}^V_{(q)}}\big)^{-1} = (\boldsymbol{S}^{\text{eff HS}}_{p\subset q})^{-1}$ is straightforward:

$$\begin{aligned} f_p\big(\boldsymbol{C}^q-\boldsymbol{C}^{\text{eff HS}}_{p\subset q}\big)^{-1} &= \big(\boldsymbol{\Delta C}^{q|p}\big)^{-1} - f_q\overline{\boldsymbol{t}^V_{(q)}} = \boldsymbol{S}^q - \boldsymbol{S}^q:\big(\boldsymbol{\Delta S}^{q|p}\big)^{-1}:\boldsymbol{S}^q - f_q\big(\boldsymbol{S}^q-\boldsymbol{S}^q:\overline{\boldsymbol{t}'^V_{(q)}}:\boldsymbol{S}^q\big)\\ &= f_p\boldsymbol{S}^q - f_p\boldsymbol{S}^q:\big(\boldsymbol{S}^q-\boldsymbol{S}^{\text{eff HS}}_{p\subset q}\big)^{-1}:\boldsymbol{S}^q\\ &= f_p\boldsymbol{S}^q - \boldsymbol{S}^q:\big((\boldsymbol{\Delta S}^{q|p})^{-1} - f_q\overline{\boldsymbol{t}'^V_{(q)}}\big):\boldsymbol{S}^q. \end{aligned} \tag{B.1}$$

Equation (B.1) gives

$$f_p\big(\boldsymbol{S}^q-\boldsymbol{S}^{\text{eff HS}}_{p\subset q}\big)^{-1} = (\boldsymbol{\Delta S}^{q|p})^{-1} - f_q\overline{\boldsymbol{t}'^V_{(q)}}. \tag{B.2}$$

The SC estimate. For all congruent grains of two constitutive phases, on can write

$$f_p\big((\boldsymbol{C}^{\text{eff}}_{\text{SC}}-\boldsymbol{C}^p)^{-1} - \overline{\boldsymbol{t}^V_{\boldsymbol{C}\text{eff}}}\big)^{-1} + f_q\big((\boldsymbol{C}^{\text{eff}}_{\text{SC}}-\boldsymbol{C}^q)^{-1} - \overline{\boldsymbol{t}^V_{\boldsymbol{C}\text{eff}}}\big)^{-1} = 0, \tag{B.3a}$$

$$f_q\big((\boldsymbol{C}^{\text{eff}}_{\text{SC}}-\boldsymbol{C}^p)^{-1} - \overline{\boldsymbol{t}^V_{\boldsymbol{C}\text{eff}}}\big) + f_p\big((\boldsymbol{C}^{\text{eff}}_{\text{SC}}-\boldsymbol{C}^q)^{-1} - \overline{\boldsymbol{t}^V_{\boldsymbol{C}\text{eff}}}\big) = 0. \tag{B.3b}$$

Equation (B.3b) yields $\overline{\boldsymbol{t}^V_{\boldsymbol{C}\text{eff}}} = f_q\big((\boldsymbol{C}^{\text{eff}}_{\text{SC}}-\boldsymbol{C}^p)^{-1}\big) + f_p\big((\boldsymbol{C}^{\text{eff}}_{\text{SC}}-\boldsymbol{C}^q)^{-1}\big)$. Further simple manipulations yield the SC approximation form of (16) for general (a,b) phases. A similar form is obtained in terms of the corresponding compliances, using the stress Green operators $\boldsymbol{t}'$. One verifies that $\boldsymbol{S}^{\text{eff}}_{\text{SC}} = (\boldsymbol{C}^{\text{eff}}_{\text{SC}})^{-1}$ simply using the platelet decompositions of both operators, which in that case refer to the same reference material, unlike the IPS estimate.

Appendix C. The IFS, IPS and ISC effective shear moduli in isotropic incompressible elasticity

For x_3-oriented fibers, the two shear moduli of the HS bounds read from (3), with $\eta = (1-2\nu_b)/(2-2\nu_b)$:

$$\mu_{1212}{}^{*F(\omega)}_{a\subset b} = \mu_b - c_a\left(\frac{1}{\mu_b-\mu_a} - \frac{c_b}{2\mu_b}(1+\eta)\right)^{-1}, \quad \mu_{i3i3}{}^{*F(\omega)}_{a\subset b} = \mu_b - c_a\left(\frac{1}{\mu_b-\mu_a} - c_b\frac{1}{2\mu_b}\right)^{-1}.$$

The two IFS moduli can be calculated with the coefficients of Table 2 and the moduli of the x_3-oriented fiber system, or at least appropriate partial sums. For the IFS shear modulus, we need the two shear moduli and

$$\Sigma = \tfrac{1}{15}(C_{iiii} + C_{3333} - 2C_{ii33})^{*F(\omega)}_{a\subset b}.$$

In the incompressible case, $\eta = 0$, the two shear moduli are equal and

$$\Sigma = \frac{1}{15}\left(4\mu_b - c_a(\mu_b - \mu_a)\frac{(5\mu_b + 3\{\mu\})}{(\mu_b + \{\mu\})}\right),$$

which gives, from (14),

$$\mu^{\text{eff IFS}}_{a\subset b} = \tfrac{11}{15}\mu^{*F(\omega)}_{a\subset b} + \Sigma = \frac{\mu_b}{15}\left(4 + 11\left(\frac{\mu_a + \langle\mu\rangle}{\mu_a + \{\mu\}}\right)\right) - \frac{c_a(\mu_b - \mu_a)}{15}\frac{(5\mu_b + 3\{\mu\})}{(\mu_b + \{\mu\})}. \tag{C.1}$$

For the IPS estimate in the incompressible case, one has, directly from (15),

$$\mu^{\text{eff IPS}}_{a,b} = \langle\mu\rangle + \frac{4\big(\{\mu\} - \mu^a\big)\big(\{\mu\} - \mu^b\big)}{10\{\mu\}} = \frac{3}{5}\langle\mu\rangle + \frac{2}{5}\frac{\mu^a\mu^b}{\{\mu\}}. \tag{C.2}$$

For comparison, the IHS and the ISC shear moduli estimate read, still with incompressibility,

$$\mu^{\text{eff IHS}}_{a\subset b} = \mu_b - c_a\left(\frac{1}{\mu_b - \mu_a} - \frac{2c_b}{5\mu_b}\right)^{-1} = \mu_b\left(\frac{2\mu_a + 3\langle\mu\rangle}{3\mu_b + 2\{\mu\}}\right), \tag{C.3}$$

$$\mu^{\text{eff ISC}}_{a,b} = \langle\mu\rangle + \frac{4\big(\mu^{\text{eff}}_{S-C} - \mu^a\big)\big(\mu^{\text{eff}}_{S-C} - \mu^b\big)}{10\mu^{\text{eff}}_{S-C}} = \tfrac{1}{6}\big(\sqrt{B^2 + 24\mu^a\mu^b} - B\big), \quad \text{with } B = 2\{\mu\} - 3\langle\mu\rangle. \tag{C.4}$$

For the IFS(ϕ) estimates (18), the first dilution of an embedded phase (a) fraction $\kappa_a = (1-\phi_a)c_a$ in phase (b) (resp. b in a) yields from (C.3) a modified phase $\breve{b}$ of shear modulus $\breve{\mu}_b$ (resp. $\breve{\mu}_a$ for $\breve{a}$). The concentration of phase (b) changes from $c_b = 1 - c_a$ to $1 - \kappa_a \neq \kappa_b$. The second dilution of infinite fibers yields $\mu^{\text{eff IFS}(\phi)}_{a\subset b} = \mu^{\text{eff IFS}}_{a\subset b}$ from (C.1) with $\breve{c}_a = (c_a - \kappa_a)/(1-\kappa_a)$ (resp. $\breve{c}_b$ for $\mu^{\text{eff IFS}(\phi)}_{b\subset a} = \mu^{\text{eff IFS}}_{b\subset a}$). The matrix with $\breve{c}_a$ fiber fraction has concentration $1 - \breve{c}_a \neq \breve{c}_b$. The dual IPS estimate from the compliance integral in (11b) reads, when incompressible,

$$\frac{1}{\mu^*} = \left\langle\frac{1}{\mu}\right\rangle + \left(\left\{\frac{1}{\mu}\right\} - \frac{1}{\mu_a}\right)\frac{5\tilde{B} - 4\tilde{A}}{15\tilde{B}^2}\left(\left\{\frac{1}{\mu}\right\} - \frac{1}{\mu_b}\right) = \left\langle\frac{1}{\mu}\right\rangle + \left(\left\{\frac{1}{\mu}\right\} - \frac{1}{\mu_a}\right)\frac{3}{5\tilde{B}}\left(\left\{\frac{1}{\mu}\right\} - \frac{1}{\mu_b}\right),$$

with $\tilde{B} = \left\{\dfrac{1}{\mu}\right\} = \dfrac{\langle\mu\rangle}{\mu_a\mu_b}$ for the reference medium. Hence

$$\mu^{\text{eff IPS(dual)}}_{a,b} = \frac{\langle\mu\rangle}{1 + \dfrac{2c_ac_b(\mu_a - \mu_b)^2}{5\mu_a\mu_b}}$$

This estimate is very close to the lower HS bound and out of the IFS sup limits.

When phase (a) is void, all these estimates equal μ_b at $c_b = 1$ and for $c_b \in [0, 1[$ they become

$$\mu_{0\subset b}^{\text{eff IFS}} = \frac{(5+c_a)c_b\mu_b}{5(1+c_a)}, \quad \mu_{b\subset 0}^{\text{eff IFS}} = \frac{c_b\mu_b}{5}, \quad \mu_{0,b}^{\text{eff IPS}} = \frac{3c_b\mu_b}{5}, \quad \mu_{0\subset b}^{\text{eff IHS}} = \frac{3c_b\mu_b}{3+2c_a},$$
$$\mu_{b\subset 0}^{\text{eff IHS}} = 0, \quad \mu_{0,b}^{\text{eff IPS(dual)}} = 0, \quad \mu_{0,b}^{\text{eff ISC}} = \begin{cases} 0 & \text{for } c_b \in \left[0, \frac{2}{5}\right], \\ \dfrac{5c_b-2}{3}\mu_b & \text{for } c_b \in \left[\frac{2}{5}, 1\right], \end{cases} \tag{C.5}$$
$$\mu_{0\subset b}^{\text{eff IFS}(\phi)} = \frac{(5+\check{c}_a)(1-\check{c}_a)\check{\mu}_b}{5(1+\check{c}_a)} = \frac{(5+\check{c}_a)(1-\check{c}_a)}{5(1+\check{c}_a)}\frac{3(1-\kappa_a)\mu_b}{3+2\kappa_a}; \quad \mu_{b\subset 0}^{\text{eff IFS}(\phi)} = \frac{\check{c}_b\mu_b}{5}.$$

In the second estimate of (C.5), the lower limit, the first dilution of phase (b) in void phase is lost. The general IPF–IFS(ϕ) and ISC–IFS(ϕ) estimates when one material phase (p or q) is void have analytical forms from using the moduli of (C.5) expressed for the phase pair (p, q) and concentrations f_p, f_q as the moduli of the intermediate homogeneous equivalent media (a) and (b) in (C.2) and (C.4), respectively, making use of (20a) and (20b) for c_a and for the two ϕ_p, ϕ_q functions defining $\check{c}_p$, κ_p and $\check{c}_q$, κ_q in (C.5). For the ISCP estimate when phase (a) is void $\mu_{0,b}^{\text{eff ISCP}}$ must satisfy

$$\frac{4\mu^*}{3} + \frac{2\mu^*(\mu^* - f_b\mu_b)}{3\mu^* + 2f_b\mu_b} = 0,$$

the (not reported) resolution giving $\mu_{0,b}^{\text{eff ISCP}} = \mu^* = 0$ for all f_b.

References

[Agrawal et al. 2003] P. Agrawal, K. Conlon, K. J. Bowman, C. T. Sun, F. R. Cichocki, Jr., and K. P. Trumble, "Thermal residual stresses in co-continuous composites", *Acta Mater.* **51**:4 (2003), 1143–1156.

[Berk 1987] N. F. Berk, "Scattering properties of a model bicontinuous structure with a well defined length scale", *Phys. Rev. Lett.* **58**:25 (1987), 2718–2721.

[Berryman 1985] J. G. Berryman, "Variational bounds on elastic constants for the penetrable sphere model", *J. Phys. D Appl. Phys.* **18**:4 (1985), 585–597.

[Boucher 1974] S. Boucher, "On the effective moduli of isotropic two-phase elastic composites", *J. Compos. Mater.* **8**:1 (1974), 82–89.

[Brenner et al. 2009] R. Brenner, R. A. Lebensohn, and O. Castelnau, "Elastic anisotropy and yield surface estimates of polycrystals", *Int. J. Solids Struct.* **46**:16 (2009), 3018–3026.

[Bretheau et al. 1988] T. Bretheau, D. Caldemaison, A. Feylessoufi, J. P. Fondère, and A. Zaoui, "Plasticity and space distribution of the phases in iron/silver two-phase material", *J. Mater. Sci.* **23**:11 (1988), 4022–4026.

[Burt and Korren 1996] M. Burt and A. Korren, "Periodic hyperbolic surfaces and subdivision of 3-space", pp. 179–183 in *Katachi U symmetry* (Tsukuba, 1994), edited by T. Ogawa et al., Springer, Tokyo, 1996.

[Chen et al. 2008] J. Chen, L. Xu, and H. Li, "Investigation on a direct modeling strategy for the effective elastic moduli prediction of composite material", *Mater. Sci. Eng. A* **491**:1–2 (2008), 385–389.

[Cherkaev 2000] A. Cherkaev, *Variational methods for structural optimization*, Applied Mathematical Sciences **140**, Springer, New York, 2000.

[Christensen 1979a] R. M. Christensen, *Mechanics of composite materials*, Wiley, New York, 1979.

[Christensen 1979b] R. M. Christensen, "Isotropic properties of platelet-reinforced media", *J. Eng. Mater. Technol.* (*ASME*) **101**:3 (1979), 299–303.

[Christensen and Waals 1972] R. M. Christensen and F. M. Waals, "Effective stiffness of randomly oriented fibre composites", *J. Compos. Mater.* **6**:3 (1972), 518–535.

[Dalmaz et al. 2000] A. Dalmaz, D. Ducret, R. El Guerjouma, P. Reynaud, P. Franciosi, D. Rouby, G. Fantozzi, and J. C. Baboux, "Elastic moduli of a 2.5D C/SiC composite: experimental and theoretical estimates", *Compos. Sci. Technol.* **60**:6 (2000), 913–925.

[DeBartolo and Hillberry 1998] E. A. DeBartolo and B. M. Hillberry, "Effects of constituent particle clusters on fatigue behavior of 2024-T3 aluminum alloy", *Int. J. Fatigue* **20**:10 (1998), 727–735.

[Delannay et al. 2006] L. Delannay, F. Lani, T. Pardoen, and F. Delannay, "Mean field modelling of the plastic behaviour of co-continuous dual-phase alloys with strong morphological anisotropy", *Int. J. Plast.* **22**:12 (2006), 2327–2345.

[Dendievel et al. 2002] R. Dendievel, J. J. Blandin, M. Fivel, M. Audier, and M. Duneau, "Mechanical properties of composites with an icosahedral fibre packing reinforcement", *Philos. Mag. A* **82**:14 (2002), 2631–2653.

[El Omri et al. 2000] A. El Omri, A. Fennan, F. Sidoroff, and A. Hihi, "Elastic-plastic homogenization for layered composites", *Eur. J. Mech. A Solids* **19**:4 (2000), 585–601.

[Errabii et al. 2007] A. Errabii, A. El Omri, and P. Franciosi, "Layered-based bounding for effective properties of elastic materials", pp. 293–294 in *8éme Congrès de Mécanique* (El Jadida, 2007), vol. 1, 2007.

[Estevez et al. 1999] R. Estevez, E. Maire, P. Franciosi, and D. S. Wilkinson, "Effect of particle clustering on the strengthening versus damage rivalry in particulate reinforced elastic plastic materials: a 3-D analysis from a self-consistent modelling", *Eur. J. Mech. A Solids* **18**:5 (1999), 785–804.

[Fan 1995] Z. Fan, "A new approach to the electrical resistivity of two-phase composites", *Acta Metall. Mater.* **43**:1 (1995), 43–49.

[Feng et al. 2003] X.-Q. Feng, Y.-W. Mai, and Q.-H. Qin, "A micromechanical model for interpenetrating multiphase composites", *Comput. Mater. Sci.* **28**:3–4 (2003), 486–493.

[Franciosi 2005] P. Franciosi, "On the modified Green operator integral for polygonal, polyhedral and other non-ellipsoidal inclusions", *Int. J. Solids Struct.* **42**:11–12 (2005), 3509–3531.

[Franciosi 2010] P. Franciosi, "The boundary-due terms in the Green operator of inclusion patterns from distant to contact and to connected situations using radon transforms: illustration for spheroid alignments in isotropic media", *Int. J. Solids Struct.* **47**:2 (2010), 304–319.

[Franciosi and Berbenni 2007] P. Franciosi and S. Berbenni, "Heterogeneous crystal and poly-crystal plasticity modeling from a transformation field analysis within a regularized Schmid law", *J. Mech. Phys. Solids* **55**:11 (2007), 2265–2299.

[Franciosi and Berbenni 2008] P. Franciosi and S. Berbenni, "Multi-laminate plastic-strain organization for non-uniform TFA modeling of poly-crystal regularized plastic flow", *Int. J. Plast.* **24**:9 (2008), 1549–1580.

[Franciosi and El Omri 2011] P. Franciosi and A. El Omri, "Effective properties of fiber and platelet systems and related phase arrangements in n-phase heterogeneous media", *Mech. Res. Commun.* **38**:1 (2011), 38–44.

[Franciosi and Lormand 2004] P. Franciosi and G. Lormand, "Using the radon transform to solve inclusion problems in elasticity", *Int. J. Solids Struct.* **41**:3–4 (2004), 585–606.

[Gel'fand et al. 1966] I. M. Gel'fand, M. I. Graev, and N. Y. Vilenkin, *Generalized functions, 5: Integral geometry and representation theory*, Academic Press, New York, 1966.

[Gent and Thomas 1959] A. N. Gent and A. G. Thomas, "The deformation of foamed elastic materials", *J. Appl. Polym. Sci.* **1**:1 (1959), 107–113.

[Gong et al. 2005] L. Gong, S. Kyriakides, and W.-Y. Jang, "Compressive response of open-cell foams, I: Morphology and elastic properties", *Int. J. Solids Struct.* **42**:5–6 (2005), 1355–1379.

[Hashin 1979] Z. Hashin, "Analysis of properties of fiber composites with anisotropic constituents", *J. Appl. Mech.* (*ASME*) **46**:3 (1979), 543–550.

[Hashin 1983] Z. Hashin, "Analysis of composite materials: a survey", *J. Appl. Mech.* (*ASME*) **50**:3 (1983), 481–505.

[Hashin and Shtrikman 1963] Z. Hashin and S. Shtrikman, "A variational approach to the theory of elastic behaviour of multiphase materials", *J. Mech. Phys. Solids* **11**:2 (1963), 127–140.

[Helsing 1993] J. Helsing, "Higher-order bounds on the conductivity of composites from symmetry considerations", *Proc. R. Soc. Lond. A* **443**:1918 (1993), 451–455.

[Hill 1952] R. Hill, "The elastic behaviour of a crystalline aggregate", *Proc. Phys. Soc. A* **65**:5 (1952), 349–354.

[Hill 1965] R. Hill, "Continuum micro-mechanics of elastoplastic polycrystals", *J. Mech. Phys. Solids* **13**:2 (1965), 89–101.

[Kanaun 2003] S. K. Kanaun, "Dielectric properties of matrix composite materials with high volume concentrations of inclusions (effective field approach)", *Int. J. Eng. Sci.* **41**:12 (2003), 1287–1312.

[Kerner 1956] E. H. Kerner, "The elastic and thermo-elastic properties of composite media", *Proc. Phys. Soc. B* **69**:8 (1956), 808–813.

[Kinney et al. 2005] J. H. Kinney, J. S. Stölken, T. S. Smith, J. T. Ryaby, and N. E. Lane, "An orientation distribution function for trabecular bone", *Bone* **36**:2 (2005), 193–201.

[Ko 1965] W. L. Ko, "Deformation of foamed elastomers", *J. Cell. Plast.* **1**:1 (1965), 45–50.

[Kocks et al. 1991] U. F. Kocks, P. Franciosi, and M. Kawai, "A forest model of latent hardening and its application to polycrystal deformations", *Texture. Microstruct.* **14–18** (1991), 1103–1114.

[La Vecchia et al. 2003] G. M. La Vecchia, C. Badini, D. Puppo, and F. D'Errico, "Co-continuous Al/Al_2O_3 composite produced by liquid displacement reaction: relationship between microstructure and mechanical behavior", *J. Mater. Sci.* **38**:17 (2003), 3567–3577.

[Lebensohn et al. 2008] R. A. Lebensohn, R. Brenner, O. Castelnau, and A. D. Rollett, "Orientation image-based micromechanical modelling of subgrain texture evolution in polycrystalline copper", *Acta Mater.* **56**:15 (2008), 3914–3926.

[Lee and Gurland 1978] H. C. Lee and J. Gurland, "Hardness and deformation of cemented tungsten carbide", *Mater. Sci. Eng.* **33**:1 (1978), 125–133.

[Lefebvre et al. 2006] L.-P. Lefebvre, A. Blouin, S.-M. Rochon, and M. N. Bureau, "Elastic response of titanium foams during compression tests and using laser-ultrasonic probing", *Adv. Eng. Mater.* **8**:9 (2006), 841–846.

[Leßle et al. 1999] P. Leßle, M. Dong, and S. Schmauder, "Self-consistent matricity model to simulate the mechanical behaviour of interpenetrating microstructures", *Comput. Mater. Sci.* **15**:4 (1999), 455–465.

[Martin et al. 2003] C. L. Martin, D. Bouvard, and S. Shima, "Study of particle rearrangement during powder compaction by the discrete element method", *J. Mech. Phys. Solids* **51**:4 (2003), 667–693.

[Marur 2005] P. R. Marur, "Effective elastic moduli of syntactic foams", *Mater. Lett.* **59**:14–15 (2005), 1954–1957.

[Menges and Knipschild 1975] G. Menges and F. Knipschild, "Estimation of mechanical properties for rigid polyurethane foams", *Polym. Eng. Sci.* **15**:8 (1975), 623–627.

[Michel et al. 2001] J. C. Michel, H. Moulinec, and P. Suquet, "A computational scheme for linear and non-linear composites with arbitrary phase contrast", *Int. J. Numer. Methods Eng.* **52**:1–2 (2001), 139–160.

[Morgan et al. 2003] E. F. Morgan, H. H. Bayraktar, and T. M. Keaveny, "Trabecular bone modulus-density relationships depend on anatomic site", *J. Biomech.* **36**:7 (2003), 897–904.

[Moulinec and Suquet 1998] H. Moulinec and P. Suquet, "A numerical method for computing the overall response of nonlinear composites with complex microstructure", *Computer Methods in Applied Mechanics and Engineering* **157**:1-2 (1998), 69–94.

[Mow and Huiskes 2004] V. C. Mow and R. Huiskes (editors), *Basic orthopaedic biomechanics & mechano-biology*, 3rd ed., Lippincott Williams & Wilkins, Philadelphia, 2004.

[Natterer 1986] F. Natterer, *The mathematics of computerized tomography*, Teubner, Stuttgart, 1986.

[Nieh et al. 1998] T. G. Nieh, J. H. Kinney, J. Wadsworth, and A. J. C. Ladd, "Morphology and elastic properties of aluminum foams produced by a casting technique", *Scr. Mater.* **38**:10 (1998), 1487–1494.

[Pavese et al. 2007] M. Pavese, M. Valle, and C. Badini, "Effect of porosity of cordierite preforms on microstructure and mechanical strength of co-continuous ceramic composites", *J. Eur. Ceram. Soc.* **27**:1 (2007), 131–141.

[Postma 1955] G. W. Postma, "Wave propagation in a stratified medium", *Geophys.* **20**:4 (1955), 780–806.

[Ramm and Katsevich 1996] A. G. Ramm and A. I. Katsevich, *The radon transform and local tomography*, CRC Press, Boca Raton, FL, 1996.

[Ravichandran 1994] K. S. Ravichandran, "Deformation behavior of interpenetrating-phase composites", *Compos. Sci. Technol.* **52**:4 (1994), 541–549.

[Ricotti et al. 2006] Y. Ricotti, D. Ducret, R. El Guerjouma, and P. Franciosi, "Anisotropy of hygrothermal damage in fiber/polymer composites: effective elasticity measures and estimates", *Mech. Mater.* **38**:12 (2006), 1143–1158.

[Roberts and Garboczi 2002] A. P. Roberts and E. J. Garboczi, "Computation of the linear elastic properties of random porous materials with a wide variety of microstructure", *Proc. R. Soc. Lond. A* **458**:2021 (2002), 1033–1054.

[Serra 1982] J. Serra, *Image analysis and mathematical morphology*, Academic Press, London, 1982.

[Singh et al. 2008] H. Singh, A. M. Gokhale, S. I. Lieberman, and S. Tamisirakandala, "Image based computations of lineal path probability distributions for microstructure representation", *Mater. Sci. Eng. A* **474**:1–2 (2008), 104–111.

[Torquato 2002] S. Torquato, *Random heterogeneous materials: microstructure and macroscopic properties*, Interdisciplinary Applied Mathematics **16**, Springer, New York, 2002.

[Veenstra et al. 2000] H. Veenstra, P. C. J. Verkooijen, B. J. J. van Lent, J. van Dam, A. P. de Boer, and A. H. J. Nijhof, "On the mechanical properties of co-continuous polymer blends: experimental and modelling", *Polymer* **41**:5 (2000), 1817–1826.

[Walpole 1978] L. J. Walpole, "A coated inclusion in an elastic medium", *Math. Proc. Cambridge Philos. Soc.* **83**:3 (1978), 495–506.

[Walpole 1981] L. J. Walpole, "Elastic behavior of composite materials: theoretical foundations", *Adv. Appl. Mech.* **21** (1981), 169–242.

[Warren and Kraynik 1987] W. E. Warren and A. M. Kraynik, "Foam mechanics: the linear elastic response of two-dimensional spatially periodic cellular materials", *Mech. Mater.* **6**:1 (1987), 27–37.

[Warren and Kraynik 1997] W. E. Warren and A. M. Kraynik, "Linear elastic behavior of a low-density Kelvin foam with open cells", *J. Appl. Mech.* (*ASME*) **64**:4 (1997), 787–794.

[Zeller and Dederichs 1973] R. Zeller and P. H. Dederichs, "Elastic constants of polycrystals", *Phys. Status Solidi B* **55**:2 (1973), 831–842.

Received 19 Jun 2010. Revised 28 Nov 2010. Accepted 19 Dec 2010.

PATRICK FRANCIOSI: patrick.franciosi@univ-paris13.fr
LPMTM, UPR9001 CNRS, Institut Galilée, Université Paris 13, 93430 Villetaneuse, France

RENALD BRENNER: renald.brenner@univ-paris13.fr
LPMTM, UPR9001 CNRS, Institut Galilée, Université Paris 13, 93430 Villetaneuse, France

ABDERRAHIM EL OMRI: abderrahim_elomri@yahoo.fr
L M M, Faculté des Sciences et Techniques de Tanger, BP 416, Tanger, Morocco

JOURNAL OF MECHANICS OF MATERIALS AND STRUCTURES

jomms.org

Founded by Charles R. Steele and Marie-Louise Steele

See http://jomms.org for submission guidelines.

JoMMS (ISSN 1559-3959) is published in 10 issues a year. The subscription price for 2011 is US $520/year for the electronic version, and $690/year (+$60 shipping outside the US) for print and electronic. Subscriptions, requests for back issues, and changes of address should be sent to Mathematical Sciences Publishers, Department of Mathematics, University of California, Berkeley, CA 94720–3840.

JoMMS peer-review and production is managed by EditFLOW™ from Mathematical Sciences Publishers.

PUBLISHED BY

mathematical sciences publishers

http://msp.org/

A NON-PROFIT CORPORATION

Typeset in LaTeX

Journal of Mechanics of Materials and Structures

Volume 6, No. 5 May 2011